DALTON
FULL PAPER

Solid state coordination chemistry of the copper(I)–cyano–organodiimine system. Two- and three-dimensional copper cyanide phases incorporating linear dipodal ligands

Douglas J. Chesnut, Dan Plewak and Jon Zubieta *

Department of Chemistry, Syracuse University, Syracuse, New York, 13244, USA

Received 3rd January 2001, Accepted 20th June 2001
First published as an Advance Article on the web 21st August 2001

A series of composite inorganic–organic materials from the copper/cyanide/organoimine system have been isolated and structurally characterized. The structural consequences of introducing sterically demanding substituents and of expanding the donor to donor distance in linear dipodal organodiimine ligands has been addressed, exploiting the bridging bidentate ligands pyrazine (pyr), 2-methylpyrazine (mpyr), 2-ethylpyrazine (etpyr), 2,3-dimethylpyrazine (2,3-dmp), 2,5-dimethylpyrazine (2,5-dmp), 2,6-dimethylpyrazine (2,6-dmp), quinoxaline (qox), phenazine (phenz), 4,4′-bipyridine (4,4′-bpy) and *trans*-4,4′-bipyridylethylene (dpe). Hydrothermal reactions of CuCN and KCN with the appropriate ligand yielded two general subclasses of materials: two-dimensional networks and three-dimensional frameworks. The 2-D phases include $[Cu_3(CN)_3(pyr)]$ (**1**), $[Cu_2(CN)_2(etpyr)]$ (**2**), $[Cu_2(CN)_2(tmp)]$ (**3**), $[Cu_2(CN)_2(qox)]$ (**4**), $[Cu_2(CN)_2(phenz)]$ (**5**) and $[Cu_7(CN)_7(4,4'\text{-bpy})_2]$ (**6**). The 3-D materials are represented by $[Cu_3(CN)_3(pyr)_2]$ (**7**), $[Cu_2(CN)_2(mpyr)]$ (**8**), $[Cu_2(CN)_2(2,3\text{-dmp})]$ (**9**), $[Cu_2(CN)_2(2,5\text{-dmp})]$ (**10**), $[Cu_2(CN)_2(2,6\text{-dmp})]$ (**11**), $[Cu_2(CN)_2(4,4'\text{-bpy})]$(**12**) and $[Cu_2(CN)_2(dpe)]$ (**13**). The materials characteristically exhibit $\{Cu(CN)\}_n$ chains and/or $\{Cu_x(CN)_x\}$ rings as structural motifs. The detailed connectivity between such substructures is influenced by the identity of the organodiimine ligand and the associated steric demands and spatial extension. The syntheses and structural characterization by X-ray diffraction of **1**–**13** are discussed in relation to the supramolecular chemistry of other copper cyanide solid state materials.

Introduction

Transition metal cyanides[1,2] are of considerable contemporary interest as inclusion compounds,[3] composite inorganic–organic zeolitic materials,[4,5] catalysts,[6] and high-T_c molecular-based magnets.[7,8] In the specific case of copper(I) cyanide,[9] applications in cyano-Gilman chemistry,[10] to the construction of network and open-framework materials,[11–15] and as precursors in the preparation of superconducting materials[16] have been noted.

Our approach to the copper cyanide system derives from an interest in the designed construction of coordination polymers[17,18] whose structures are dictated by an interplay of metal coordination preferences and the donor group dispositions and steric demands of the ligands. The ultimate goal is to exploit such structural characteristics of both the metal and the ligand to control the topological characteristics of the composite material and thus influence the physical properties of the materials. The copper cyanide system is particularly attractive from this viewpoint by virtue of the versatility of $\{Cu_x(CN)_y\}_n$ substructures in accommodating various ligand-imposed geometric requirements.[19,20] A variety of chain and network structures have been described for the Cu(I) cyanide system with simple chelating ligands such as 2,2′-bipyridine and bis-2,3-(2-pyridyl)pyrazine and with the bridging tridentate ligand 1,2,4-triazolate.[12–15]

As an extension of these studies, the chemistry of copper(I) cyanide with a series of bridging dipodal ligands, shown in Scheme 1 was investigated. For the prototypical ligand of the set, pyrazine, the consequences of the steric constraints imposed by substituents were explored in the ligand set 2-methylpyrazine (mpyr), 2-ethylpyrazine (etpyr), 2,3-dimethylpyrazine (2,3-dmp), 2,5-dimethylpyrazine (2,5-dmp), 2,6-dimethylpyrazine (2,6-dmp), quinoxaline (qox), and phenazine (phenz). The effects of spatial extension between imine donor groups were addressed by introducing 4,4′-bipyridine (4,4′-bpy) and *trans*-4,4′-bipyridylethylene (dpe). The hydrothermal chemistry of Cu(CN) with these ligands resulted in the isolation and characterization of the two-dimensional phases $[Cu_3(CN)_3(pyr)]$ (**1**), $[Cu_2(CN)_2(etpyr)]$ (**2**), $[Cu_2(CN)_2(tmp)]$ (**3**),

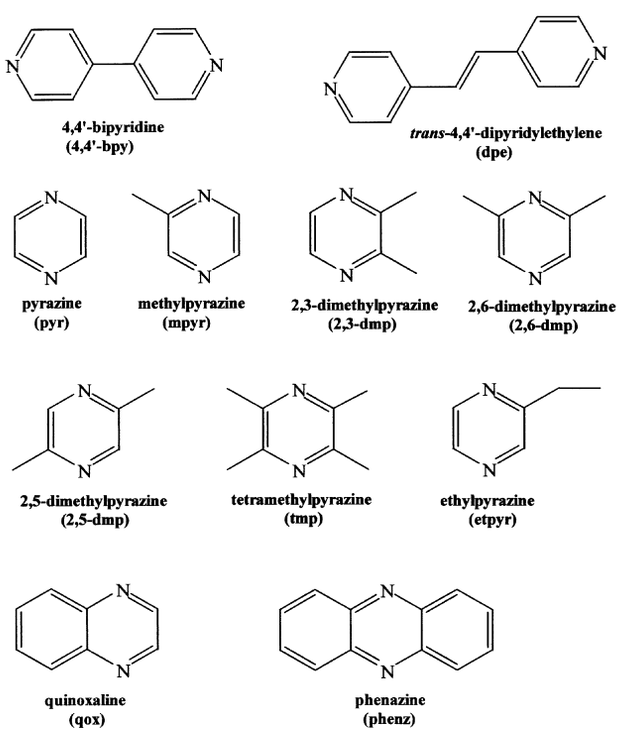

Scheme 1

$[Cu_2(CN)_2(qox)]$ (**4**), $[Cu_2(CN)_2(phenz)]$ (**5**) and $[Cu_7(CN)_7(4,4'\text{-bpy})_2]$ (**6**) and of the framework materials $[Cu_3(CN)_3(pyr)_2]$ (**7**), $[Cu_2(CN)_2(mpyr)]$ (**8**), $[Cu_2(CN)_2(2,3\text{-dmp})]$ (**9**), $[Cu_2(CN)_2(2,5\text{-dmp})]$ (**10**), $[Cu_2(CN)_2(2,6\text{-dmp})]$ (**11**), $[Cu_2(CN)_2(4,4'\text{-bpy})]$ (**12**) and $[Cu_2(CN)_2(dpe)]$ (**13**). While this work was in progress the structure of $[Cu_2(CN)_2(mpyr)]$ was described elsewhere.[19]

Experimental

Reagents were purchased from Aldrich Chemical Co. and used without further purification. All syntheses were carried out in 23 mL polytetrafluoroethylene-lined Parr stainless steel containers under autogenous pressure. The reactants were stirred briefly before heating. Water was distilled above 3.0 Ω in-house using a Barnstead Model 525 Biopure Distilled Water Center.

Syntheses

$[Cu_3(CN)_3(pyr)]$ (1) and $[Cu_3(CN)_3(pyr)_2]$ (7). $[Cu_3(CN)_3(pyr)]$ (**1**) and $[Cu_3(CN)_3(pyr)_2]$ (**7**) were prepared as yellow-orange lamellar crystals and yellow needles, respectively, from the hydrothermal reaction of CuCN (0.363 g, 4.05 mmol), KCN (0.063 g, 0.97 mmol), pyr (0.080 g, 1.0 mmol), and H_2O (5.00 mL, 0.278 mol) in a Parr acid digestion vessel of 23 mL volume. The reagents were added to the reaction vessel in the order listed and heated at 180 ± 5 °C for 125 h. Upon overnight cooling to room temperature, a mixture of small needle-like orange crystals of **7** and lamellar yellow crystals of **1** were recovered in 40% total yield. Attempts to prepare monophasic samples of **1** and **7** under hydrothermal conditions proved unsuccessful.

$[Cu_2(CN)_2(etpyr)]$ (2). The reaction of CuCN (0.358 g, 3.99 mmol), KCN (0.064 g, 0.98 mmol), and 5.00 mL of aqueous 0.20 mmol mL^{-1} 2-ethylpyrazine for 70.5 h at 175 ± 5 °C yielded long yellow needles of **2** in 60% yield.

$[Cu_2(CN)_2(tmp)]$ (3). A mixture of CuCN (0.360 g, 4.02 mmol), KCN (0.066 g, 1.0 mmol), and tetramethylpyrazine (0.136 g, 0.993 mmol) in H_2O (5.00 mL, 0.278 mmol) was heated for 72 h at 175 ± 5 °C. After cooling for 4 h, lamellar orange crystals of **3** were recovered in *ca.* 45% yield.

$[Cu_2(CN)_2(qox)]$ (4). A mixture of CuCN (0.359 g, 4.01 mmol), KCN (0.065 g, 1.0 mmol), quinoxaline (0.131 g, 1.01 mmol), and H_2O (5.00 mL, 0.278 mol) was heated for 48 h at 160 ± 5 °C. Red crystals of **4** were recovered in *ca.* 20% yield from an uncharacterized amorphous brown powder.

$[(Cu_2(CN)_2(phenz)]$ (5). A mixture of CuCN (0.316 g, 4.03 mmol), KCN (0.064 g, 0.98 mmol), and phenazine (0.179 g, 0.993 mmol), in H_2O (5.00 mL, 0.278 mol) was heated for 72 h at 175 ± 5 °C. After cooling at room temperature, dark red crystals of **5** were collected in 60% yield.

$[Cu_7(CN)_7(4,4'\text{-bpy})_2]$ (6) and $[Cu_2(CN)_2(4,4'\text{-bpy})]$ (12). A mixture of CuCN (0.361 g, 4.03 mmol), KCN (0.064 g, 0.98 mmol), 1,2,4-triazole (0.069 g, 1.0 mmol), 4,4′-bipyridine (0.155 g, 0.992 mmol), and H_2O (10.00 mL, 0.556 mol) was heated at 180 ± 5 °C for 72 h in a heavy wall borosilicate tube with 0.5 in inner diameter (30% charge volume). After cooling, a mixture of orange crystals of **12** and prismatic yellow crystals of **6** was recovered. Attempts to prepare monophasic samples of **6** and **12** under a variety of hydrothermal conditions proved unsuccessful. Curiously, the reagent 1,2,4-triazole was necessary for the isolation of crystalline materials.

$[Cu_2(CN)_2(mpyr)]$ (8). Yellow crystals of **8** were prepared in 70% yield from the hydrothermal reactions of CuCN (0.358 g, 4.00 mmol), KCN (0.064 g, 0.99 mmol), and 5.00 mL of 0.20 mmolar aqueous 2-methylpyrazine at 175 ± 5 °C for 22 h.

$[Cu_2(CN)_2(2,3\text{-dmp})]$ (9). A mixture of CuCN (0.357 g, 3.98 mmol), KCN (0.068 g, 1.0 mmol), and 5.00 mL of a 0.20 mmolar aqueous solution of 2,3-dimethylpyrazine was heated at 175 ± 5 °C for 24 h. Yellow crystals of **9** were isolated in 40% yield.

$[Cu_2(CN)_2(2,5\text{-dmp})]$ 10. Light yellow crystals of **10** were prepared in *ca.* 25% yield from the reaction of a mixture of CuCN (0.358 g, 4.00 mmol), KCN (0.065 g, 1.0 mmol), 2,5-dimethylpyrazine (0.108 g, 1.00 mmol), and H_2O (5.00 mL, 0.278 mol) at 175 ± 5 °C for 22 h.

$[Cu_2(CN)_2(2,6\text{-dmp})]$ (11). The reaction of a mixture of CuCN (0.363 g, 4.05 mmol), KCN (0.065 g, 1.0 mmol), 2,6-dimethylpyrazine (0.104 g, 0.963 mmol), and 5.00 mL of H_2O (0.278 mol) at 180 ± 5 °C for 95 h yielded yellow blocks of **11** in *ca.* 25% yield.

$[Cu_2(CN)_2(dpe)]$ (13). A mixture of CuCN (0.359 g, 4.01 mmol), KCN (0.066 g, 1.0 mmol), *trans*-4,4′-dipyridylethylene (0.181 g, 0.994 mmol), and H_2O (5.00 mL, 0.278 mol) was heated at 170 ± 5 °C for 96 h. After cooling to room temperature, yellow-orange crystals of **13** were recovered in *ca.* 30% yield.

Crystal structure determinations

Single crystal diffraction data for **1**–**13** were measured using a Bruker P4 diffractometer equipped with the SMART system[21] and using Mo-Kα radiation ($\lambda = 0.71073$ Å). All data sets were corrected for Lorentz and polarization effects, and absorption corrections were made using SADABS.[22] The structure solutions and refinements were carried out using SHELXL96.[23] All structures were solved using direct-methods and all of the non-hydrogen atoms were located from the initial solution or from subsequent electron density difference maps during the initial stages of the refinement. After locating all of the non-hydrogen atoms in each structure the models were refined against F^2, first using isotropic and finally anisotropic thermal displacement parameters, until the final value of σ/Δ_{max} was less than 0.001. The positions of the hydrogen atoms were then calculated and fixed, and a final cycle of refinements was performed until σ/δ_{max} was again less than 0.001. The cyano groups of all structures but **2** were disordered with respect to C and N occupancies. The locations of the C or N atoms were modeled with each position of the cyano group assigned an occupancy of 50% C and 50% N. The temperature factors were then refined simultaneously.

The crystal data for **1**–**13** are summarized in Table 1. Selected bond lengths and angles for the structures of **1**–**13** are presented in Tables 2–14.

CCDC reference numbers 156963–156975.

See http://www.rsc.org/suppdata/dt/b1/b100390i/ for crystallographic data in CIF or other electronic format.

Results

Synthesis

Traditional high-temperature methods for preparing inorganic solid state materials generally lead to the isolation of thermodynamic phases. To modify the microstructures of solid state materials, a shift to the kinetic domain is required to provide access to metastable phases.[24] A variety of *chimie douce* methods have been developed and applied to the isolation of such metastable phases, which are often inaccessible by more traditional methods.[25]

Table 1 Summary of crystallographic data for compounds **1–13**

	1	**2**	**3**	**4**	**5**	**6**	**7**	**8**	**9**	**10**	**11**	**12**	**13**
Empirical formula	$C_7H_4Cu_3N_5$	$C_8H_8Cu_2N_4$	$C_{10}H_{12}Cu_2N_4$	$C_{20}H_{12}Cu_4N_8$	$C_{14}H_8Cu_2N_4$	$C_{27}H_{16}Cu_7N_{11}$	$C_{11}H_8Cu_3N_7$	$C_7H_8Cu_2N_4$	$C_{24}H_{24}Cu_6N_{12}$	$C_8H_8Cu_2N_4$	$C_8H_8Cu_2N_4$	$C_{12}H_8Cu_2N_4$	$C_{14}H_{10}Cu_2N_4$
FW	348.77	287.26	315.32	618.54	359.32	939.29	442.86	275.53	939.29	287.26	287.26	335.50	361.34
Space group (no.)	*C*2/*c* (15)	*P*$\bar{1}$ (2)	$P2_1/n$ (14)	*P*$\bar{1}$ (2)	*Cmca* (64)	*P*$\bar{1}$ (2)	*C*2/*m* (12)	*C*2/*c* (15)	*P*$\bar{1}$ (2)	*C*2/*c* (15)	*C*2/*c* (15)	$P2_1/n$ (14)	*P*$\bar{1}$ (2)
T/K	115	115	115	115	115	115	115	115	115	115	115	115	115
a/Å	15.882(1)	7.846(3)	4.724(1)	6.843(1)	16.869(7)	7.901(2)	12.536(3)	14.122(1)	7.901(2)	14.140(3)	16.553(4)	8.487(2)	6.861(3)
b/Å	9.685(1)	9.048(3)	16.731(4)	9.605(1)	8.265(3)	8.367(2)	10.203(2)	8.726(9)	8.367(2)	8.888(1)	7.773(2)	11.444(3)	9.329(5)
c/Å	20.454(1)	14.539(6)	7.480(1)	15.589(3)	9.489(3)	11.814(3)	5.585(1)	7.250(7)	11.814(3)	7.235(1)	18.025(5)	12.591(3)	11.793(6)
α/°	90.0	76.40(1)	90.0	83.894(5)	90.0	82.367(9)	90.0	90.0	82.367(9)	90.0	90.0	90.0	97.91(1)
β/°	107.142(1)	88.06(1)	94.020(5)	81.517(5)	90.0	74.775(6)	93.544(4)	98.125	74.775(6)	97.584(4)	116.051(5)	101.033(5)	99.53(1)
γ/°	90.0	88.520(8)	90.0	71.436(5)	90.0	86.046(5)	90.0	90.0	86.046(5)	90.0	90.0	90.0	109.62(1)
V/Å^3, *Z*	2995.0(3), 12	1002.5(7), 4	587.7(2), 4	958.8(3), 2	1323.0(9), 4	746.4(3), 1	713.0(2), 2	884.6(1), 4	746.4(3), 1	901.4(3), 4	2083.5(9), 8	1214.5(5), 4	685.8(6), 2
D_c/g cm^{-3}	2.320	1.903	1.776	2.142	1.804	2.090	1.998	2.067	2.090	2.117	1.832	1.834	1.750
μ/mm^{-1}	6.299	4.204	3.582	4.404	3.206	4.930	4.435	4.759	4.930	4.675	4.045	-	3.093
												3.485	
*R*1 [a], *wR*2 [b]	0.0562, 0.1262	0.0630, 0.1205	0.0414, 0.0906	0.0498, 0.1136	0.0304, 0.0627	0.0650, 0.1543	0.0564, 0.1406	0.0356, 0.0898	0.0650, 0.1543	0.0236, 0.0625	0.0455, 0.1071	0.0259, 0.0651	0.0375, 0.1027

[a] $R1 = \Sigma||F_o| - |F_c||/\Sigma|F_o|$. [b] $wR2 = [\Sigma[w(F_o^2 - F_c^2)^2]/\Sigma[w(F_o^2)^2]]^{1/2}$.

Table 2 Bond lengths (Å) and angles (°) for $[Cu_3(CN)_3(pyr)]$ (**1**)

Cu1–X1	1.880(6)	Cu5–N11	2.136(7)
Cu2–X3A	1.861(7)	X1–X1A	1.15(1)
Cu3–X5	1.871(6)	X2–X3	1.159(8)
Cu3–X4	1.893(7)	X4–X4A	1.14(1)
Cu3–N10	2.129(6)	X5–X5A	1.18(1)
Cu4–X9A	1.868(6)	X6–X7	1.167(9)
Cu4–X6	1.876(7)	X8–X9	1.182(8)
Cu4–N12A	2.148(7)	Cu1–Cu5	2.975(2)
Cu5–X8	1.881(6)	Cu1–Cu3	2.999(2)
Cu5–X7	1.889(7)	Cu2–Cu4	2.982(1)
X2–Cu1–X1	178.0(3)	X3–Cu2–X3A	174.8(4)
X5–Cu3–X4	157.1(3)	X5–Cu3–N10	101.0(3)
X4–Cu3–N10	101.4(3)	X9A–Cu4–X6	156.5(3)
X9A–Cu4–N12A	101.2(3)	X6–Cu4–N12A	101.9(3)
X8–Cu5–X7	156.7(3)	X8–Cu5–N11	101.6(3)
X7–Cu5–N11	100.9(3)	X1A–X1–Cu1	175.5(9)
X3–X2–Cu1	176.2(6)	X2–X3–Cu2	177.9(6)
X4A–X4–Cu3	175.0(9)	X5A–X5–Cu3	173.7(9)
X6–X7–Cu5	173.7(6)	X9–X8–Cu5	172.2(6)
X8–X9–Cu4A	172.8(6)		

Table 3 Bond lengths (Å) and angles (°) for $[Cu_2(CN)_2(etpyr)]$ (**2**)

Cu1–C2A	1.868(8)	Cu3–N8	2.048(7)
Cu1–N1	1.940(7)	Cu4–C3A	1.883(8)
Cu1–N6	2.055(7)	Cu4–N4	1.944(7)
Cu2–C1	1.900(8)	Cu4–N5A	2.045(7)
Cu2–N2	1.932(7)	N1–C1	1.15(1)
Cu1–N7	2.075(7)	N2–C2	1.16(1)
Cu2–C1A	2.451(8)	N3–C3	1.14(1)
Cu2–Cu2B	2.578(2)	N4–C4	1.15(1)
Cu3–C4	1.878(8)	N5–Cu4A	2.045(7)
Cu3–N3	1.941(7)		
C2A–Cu1–N6	127.7(3)	N1–Cu1–N6	98.9(3)
C1–Cu2–N2	130.3(3)	C1–Cu2–N7	118.1(3)
N2–Cu2–N7	100.4(3)	C4–Cu3–N3	132.53
C4–Cu3–N8	126.8(3)	N3–Cu3–N8	100.1(3)
C3A–Cu4–N4	130.8(3)	C3A–Cu4–N5A	129.4(3)
N4–Cu4–N5A	99.8(3)	C1–N1–Cu1	178.7(7)
C2–N2–Cu2	171.0(7)	C3–N3–Cu3	169.3(7)
C4–N4–Cu4	170.3(7)	N1–C1–Cu2	71.4(7)
N1A–C1A–Cu2	117.1(6)	N2A–C2A–Cu1	174.4(8)
N3A–C3A–Cu4	173.1(8)	N4–C4–Cu3	173.8(7)
C2A–Cu1–N1	133.1(3)		

Of these *chimie douce*, or soft chemical, methods, reactions carried out in hydrothermal media are yielding a rich array of chemical products for a variety of systems.[26] The complexity of the hydrothermal reaction domain often allows subtle changes in reaction conditions to provide unique solid state structures. For a given chemical system, these structures are often constructed from the same or relatively similar architectural components.[27]

The syntheses of **1**–**13** exploited well-established hydrothermal methods, using conditions analogous to those employed previously for the copper(I) cyanide–organoimine ligand systems.[12–15] It is noteworthy that addition of KCN is often necessary to ensure the growth of crystals suitable for X-ray crystallography. Since the K^+ cation does not appear in the structures of these materials, we speculate that this cation may be implicated as a mineralizer or solubilizing agent in the preassembly of $\{Cu(CN)\}_\infty$ or $\{Cu(CN)_2\}_\infty^{-\infty}$ chains as precursors to the copper(I)–cyano–organoimine solids.

The materials obtained in this study contain copper exclusively in the +1 oxidation state. This observation is consistent with the thermodynamic stability of Cu(I) cyanide species with respect to Cu(II) compounds at elevated temperatures and pressures,[12–15,28] and may also reflect the stabilization of the Cu(I) oxidation state through π-backbonding to the cyano and aromatic imine ligands.[29]

Table 4 Bond lengths (Å) and angles (°) for $[Cu_2(CN)_2(tmp)]$ (**3**)

Cu1–X1	1.881(4)	Cu1–N3	2.093(3)
Cu1–X2	1.920(3)	X1–X2A	1.151(5)
X1–Cu1–N3	125.4(1)	X1–Cu1–X2	134.5(1)
X2A–X1–Cu1	176.6(3)	X2–Cu1–N3	100.1(1)
X1A–X2–Cu1	175.3(3)		

Table 5 Bond lengths (Å) and angles (°) for $[Cu_2(CN)_2(qox)]$ (**4**)

Cu1–X1	1.896(5)	Cu3–N11	2.052(4)
Cu1–X2	1.970(4)	Cu4–X8	1.872(5)
Cu1–N9	2.060(4)	Cu4–X7	1.920(4)
Cu1–Cu1A	3.032(1)	Cu4–N12A	2.170(4)
Cu2–X3	1.895(5)	N10–Cu2A	2.152(4)
Cu2–X4	1.911(4)	X1–X7	1.150(7)
Cu2–N10A	2.152(4)	X2–X3	1.150(7)
Cu3–X5	1.895(6)	X4–X5	1.159(7)
Cu3–X6	1.974(5)	X6–X8	1.164(7)
X1–Cu1–X2	123.4(2)	X1–Cu1–N9	132.1(1)
X2–Cu1–N9	102.3(1)	X3–Cu2–N10A	117.3(1)
X3–Cu2–X4	142.6(2)	X4–Cu2–N10A	99.7(1)
X5–Cu3–X6	124.4(2)	X5–Cu3–N11	134.1(2)
X6–Cu3–N11	101.1(1)	X8–Cu4–X7	144.2(2)
X8–Cu4–N12	116.6(1)	X7–Cu4–N12	98.5(1)
X7A–X1–Cu1	176.1(5)	X3–X2–Cu1	162.5(4)
X2–X3–Cu2	170.0(5)	X5–X4–Cu2	178.7(5)
X4–X5–Cu3	174.7(5)	X8–X6–Cu3	159.3(4)
X1A–X7A–Cu4	176.0(4)	X6–X8–Cu4	172.6(4)

Table 6 Bond lengths (Å) and angles (°) for $[Cu_2(CN)_2(phenz)]$ (**5**)

Cu1–X1	1.888(2)	X1–X1A	1.159(4)
Cu1–N2	2.124(3)		
X1B–Cu1–X1	146.67(1)	X1B–Cu1–N2	106.66(6)
X1–Cu1–N2	106.66(6)	X1A–X1–Cu1	176.5(2)

Table 7 Bond lengths (Å) and angles (°) for $[Cu_7(CN)_7(4,4'\text{-bpy})_2]$ (**6**)

Cu1–X2	1.88(1)	Cu4–N8	2.052(7)
Cu1–X1	1.88(1)	X1–X1A	1.16(1)
Cu2–X3	1.83(1)	X2–X3	1.24(1)
Cu3–X4	1.891(8)	X4–X4A	1.15(1)
Cu3–X5	1.875(7)	X5–X6	1.17(1)
Cu3A–N9	2.062(7)	X7–X7A	1.15(2)
Cu4–X6	1.899(8)	Cu1–Cu4A	2.620(1)
Cu4–X7	1.907(7)	Cu2–Cu3	2.950(1)
X2–Cu1–X1	156.3(4)	X3A–Cu2–X3	180.000
X5–Cu3–X4	144.4(3)	X4–Cu3–N9A	108.0(3)
X5–Cu3–N9A	106.7(3)	X6–Cu4–X7	144.7(3)
X6–Cu4–N8	108.8(3)	X7–Cu4–N8	106.5(3)
X1A–X1–Cu1	177.5(1)	X3–X2–Cu1	172.3(9)
X2–X3–Cu2	175.6(9)	X4A–X4–Cu3	175.7(1)
X6–X5–Cu3	176.5(7)	X5–X6–Cu4	175.3(7)
X7A–X7–Cu4	176.4(1)		

Table 8 Bond lengths (Å) and angles (°) for $[Cu_3(CN)_3(pyr)_2]$ (**7**)

Cu1–X1	1.919(6)	Cu2–X3	1.845(7)
Cu1–X2	1.957(7)	X1–X1A	1.17(1)
Cu1–N4	2.105(3)	X2–X3	1.14(1)
X1–Cu1–X2	128.0(2)	X1–Cu1–N4	110.3(1)
X2–Cu1–X4	103.3(1)	N4–Cu1–N4A	97.0(1)
X3–Cu2–X3A	180.0(4)	X1A–X1–Cu1	177.9(7)
X3–X2–Cu1	178.4(6)	X2–X3–Cu2	176.6(6)

Descriptions of the structures

As shown in Fig. 1, the structure of $[Cu_3(CN)_3(pyr)]$ (**1**) is constructed from one-dimensional $\{Cu(CN)\}_\infty$ chains penetrating two-dimensional $\{Cu(CN)(pyr)\}_x$ networks. The one-dimensional chains are composed of two-coordinate Cu(I) centers, Cu1 and Cu2, bridged by cyanide groups, for which the C and N termini of the bridging CN groups are crystallographically indistinguishable, a common characteristic of such structure types.[30,31] Two equivalent metal centers, Cu1, are linked by the cyanide groups X1X1A which are in turn

Table 9 Bond lengths (Å) and angles (°) for $[Cu_2(CN)_2(mpyr)]$ (**8**)

Cu1–X2A	1.914(4)	Cu1–N3	2.083(3)
Cu1–X1	1.950(3)	Cu1–X2A	2.459(4)
Cu1–Cu1A	2.568(8)	X1–X2	1.143(5)
X2A–Cu1–X1	125.8(1)	X2A–Cu1–N3	122.4(1)
X1–Cu1–N3	100.7(1)	X2A–Cu1–X2B	109.3(1)
X1–Cu1–X2A	102.1(1)	N3–Cu1–X2B	88.7(1)
X2–X1–Cu1	163.5(3)	X1–X2–Cu1	171.5(3)
X1–X2–Cu1A	115.2(3)	Cu1–X2A–Cu1A	70.7(1)

Table 10 Bond lengths (Å) and angles (°) for $[Cu_2(CN)_2(2,3\text{-dmp})]$ (**9**)

Cu1–X6A	1.888(7)	Cu5–X10	1.878(7)
Cu1–X1	1.934(6)	Cu5–X11	1.939(6)
Cu1–N18A	2.052(6)	Cu5–N17	2.048(6)
Cu2–X2	1.866(7)	Cu6–X12	1.880(7)
Cu2–X3	1.907(6)	Cu6–X7A	1.924(6)
Cu2–N13A	2.077(6)	Cu6–N15A	2.058(6)
Cu3–X4	1.896(7)	X1–X2	1.171(9)
Cu3–X5	1.941(6)	X3–X4	1.162(9)
Cu3–N14	2.101(6)	X5–X6	1.158(9)
Cu4–X8	1.898(7)	X7–X8	1.157(9)
Cu4–X9	1.947(6)	X9–X10	1.159(9)
Cu4–N16	2.105(6)	X11–X12	1.169(9)
X6A–Cu1–X1	129.4(3)	X6A–Cu1–N18A	128.2(3)
X1–Cu1–N18A	99.9(2)	X2–Cu2–X3	140.3(3)
X2–Cu2–N13A	117.7(3)	X3–Cu2–N13A	101.4(2)
X4–Cu3–X5	130.3(3)	X4–Cu3–N14	115.7(3)
X5–Cu3–N14	101.6(2)	X8–Cu4–X9	129.7(3)
X8–Cu4–N16	115.8(3)	X9–Cu4–N16	101.2(2)
X10–Cu5–X11	132.5(3)	X10–Cu5–N17	128.9(3)
X11–Cu5–N17	98.6(2)	X12–Cu6–X7A	134.3(3)
X12–Cu6–N15A	122.9(3)	X7A–Cu6–N15A	102.4(2)
X2–X1–Cu1	176.4(6)	X1–X2–Cu2	171.9(6)
X4–X3–Cu2	169.2(6)	X3–X4–Cu3	175.6(7)
X6–X5–Cu3	179.8(7)	X5A–X6A–Cu1	176.1(6)
X8A–X7A–Cu6	168.4(6)	X7–X8–Cu4	174.6(6)
X10–X9–Cu4	177.1(6)	X9–X10–Cu5	174.9(7)
X12–X11–Cu5	171.7(6)	X11–X12–Cu6	175.8(6)

Table 11 Bond lengths (Å) and angles (°) for $[Cu_2(CN)_2(2,5\text{-dmp})]$ (**10**)

Cu1–X2	1.905(2)	Cu1–X2A	2.526(2)
Cu1–X1A	1.968(1)	X1–X2	1.154(3)
Cu1–N3	2.098(1)	Cu1–Cu1A	2.6455(6)
X2–Cu1–X1A	127.24(8)	X2–Cu1–X3	124.48(8)
X1A–Cu1–N3	99.48(7)	X2–Cu1–X2A	108.23(7)
X1C–Cu1–X2A	101.07(7)	N3–Cu1–X2A	86.94(7)
X2–X1–Cu1A	164.3(1)	X1–X2–Cu1	173.8(1)

Table 12 Bond lengths (Å) and angles (°) for $[Cu_2(CN)_2(2,6\text{-dmp})]$ (**11**)

Cu1–X2	1.877(5)	Cu2–N5	2.090(4)
Cu1–X1	1.905(4)	Cu2–Cu2A	2.569(1)
Cu1–N6A	2.075(4)	X1–X4A	1.156(6)
Cu2–X4	1.903(5)	X4–Cu2A	2.434(5)
Cu2–X3	1.927(4)	X2–X3	1.147(6)
X2–Cu1–X1	138.1(1)	X2–Cu1–N6A	120.0(1)
X1–Cu1–N6A	101.4(1)	X4–Cu2–X3	132.1(1)
X4–Cu2–N5	113.3(1)	X3–Cu2–N5	101.7(1)
C4–Cu2–X4B	108.6(1)	X3–Cu2–X4B	101.4(1)
N5–Cu2–X4B	92.1(1)	X4A–X1–Cu1	172.2(4)
X3–X2–Cu1	177.2(4)	X2–X3–Cu2	170.6(4)
X1A–X4–Cu2	172.0(4)	X1A–X4–Cu2A	116.6(4)
Cu2–X4–Cu2A	71.5(1)		

Table 13 Bond lengths (Å) and angles (°) for $[Cu_2(CN)_2(4,4'\text{-bpy})]$ (**12**)

Cu1–X1	1.944(1)	Cu2–X3	1.908(1)
Cu1–X4A	1.936(2)	Cu2–N5	2.067(1)
Cu1–X4B	2.363(2)	Cu1–Cu1A	2.484(1)
Cu1–N6A	2.067(1)	X1–X2	1.155(3)
Cu2–X2	1.886(2)	X3–X4	1.149(3)
X4A–Cu1–X1	127.47(8)	X4A–Cu1–N6A	113.62(8)
X1–Cu1–N6A	106.03(8)	X4A–Cu1–X4B	110.21(7)
X1–Cu1–X4B	99.09(8)	N6A–Cu1–X4B	94.61(7)
X2–Cu2–C3	139.4(1)	X2–Cu2–N5	112.11(8)
X3–Cu2–N5	107.8(1)	X2–X1–Cu1	176.6(1)
X1–X2–Cu2	173.2(1)	X4–X3–Cu2	169.7(1)

Table 14 Bond lengths (Å) and angles (°) for $[Cu_2(CN)_2(dpe)]$ (**13**)

Cu1–X1	1.873(3)	Cu2–X3B	2.284(3)
Cu1–X2	1.912(3)	Cu2–Cu2A	2.488(1)
Cu1–N5	2.021(3)	X1–X1A	1.159(6)
Cu2–X4	1.919(3)	X2–X3	1.155(4)
Cu2–X3	1.946(3)	X4–X4C	1.152(5)
Cu2–N6B	2.071(3)		
X1–Cu1–X2	127.8(1)	X1–Cu1–N5	122.8(1)
X2–Cu1–N5	108.6(1)	X4–Cu2–X3	125.7(1)
X4–Cu2–N6B	111.1(1)	X3–Cu2–N6B	109.3(1)
X4–Cu2–X3A	102.2(1)	X3–Cu2–X3A	108.4(1)
N6B–Cu2–X3A	95.6(1)	X1A–X1–Cu1	174.4(4)
X3–X2–Cu1	168.0(2)	X2–X3–Cu2	161.6(2)
X2–X3–Cu2A	126.8(2)	Cu2–X3–Cu2A	71.6(1)
X4C–X4–Cu2	177.9(4)		

connected to Cu2 *via* an X2X3 unit (X′s refer to disordered C or N sites of the cyanide ligands). The Cu2 is subsequently bridged to another Cu2 by a second X2X3 cyanide. The Cu2 sites are rigorously linear, while Cu1 sites are not crystallographically constrained in their coordination geometry.

The network substructure of **1** involves not only two unique metal centers, Cu3 and Cu4, and four cyanide atom positions, X4–X7, but also the diimine pyrazine. The Cu(I) sites are both three-coordinate with significant deviations from the idealized trigonal geometry. Three coordination is a characteristic feature not only of Cu(I) cyanide structures such as $KCu(CN)_2$,[32] $NaCu(CN)_2{\cdot}2H_2O$,[33] and $K[Cu_2(CN)_3]{\cdot}H_2O$[34] but also of copper cyanohalide[31] and copper cyano amine structures.[35] In the structure of **1**, Cu(I) centers and cyanide ligands X4X4A, X5X6, X7X7A are arranged in coplanar $\{Cu(CN)\}_\infty$ chains. The third ligands of Cu3 and Cu4 sites are the N9 and N8 donors, respectively, of different diimine molecules. The organic molecules tie neighboring $\{Cu(CN)\}_\infty$ strands into a sheet composed of pseudohexagonal rings formulated as $\{Cu_6(CN)_4(pyr)_2\}$. The resulting 6^3 net topology[36] is shown in Fig. 1(b). Alternatively, the network may be described as $\{Cu(CN)\}_\infty$ chains linked by linear dipodal pyrazine ligands[37] into a two-dimensional sheet, constructed of $\{Cu_6(CN)_4(pyr)_2\}$ rings. The pyrazine groups are nearly coplanar with the ring plane inclined at 6°.

The$\{Cu(CN)\}_\infty$ chains incorporating Cu1 and Cu2 sites penetrate these sheets of $\{Cu_6(CN)_4(pyr)_2\}$ rings. The $\{Cu(CN)\}_\infty$ chain axis of propagation is *ca.* 48° to the sheet least square plane. Adjacent sheets stack in an offset fashion with *ca.* 2.9 Å separation, reflecting π–π interactions between pyrazine rings of adjacent sheets. While there are no Cu···Cu interactions less than 3.1 Å in length between sheets, the Cu(chain)···Cu(sheet) distances of 2.982(1), 2.975(2) and 2.999(2) Å influence the (CN)–Cu–(CN) angles of the sheets, which are considerably expanded to 156.8(3)° from the idealized trigonal planar value of 120°.

The structural consequences of introducing substituents onto the pyrazine linker are often dramatic and unpredictable, as illustrated by the structure of $[Cu_2(CN)_2(etpyr)]$ (**2**), shown in Fig. 2. The structure of **2** is constructed from one-dimensional $\{Cu(CN)\}_\infty$ chains and double-stranded $\{Cu(CN)\}_\infty$ ribbons, linked into a network by bridging ethylpyrazine ligands.

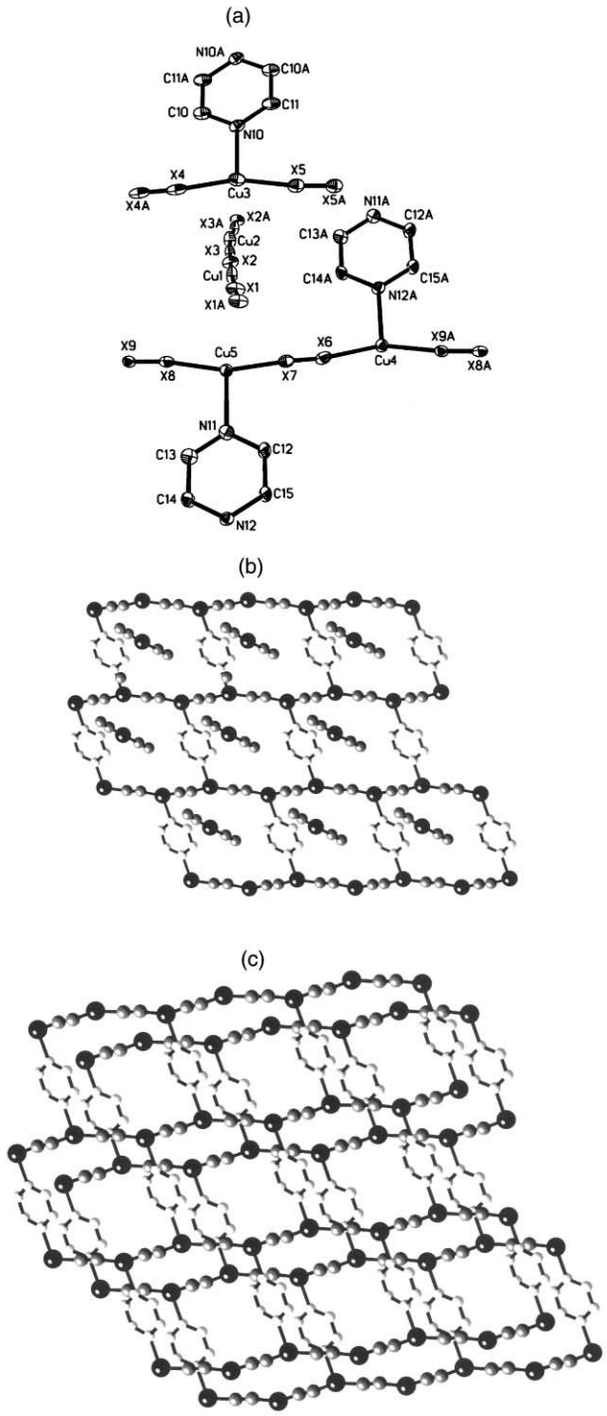

Fig. 1 (a) A view of the asymmetric unit of **1**, showing 50% thermal ellipsoids and the atom-labeling scheme. (b) A view of the penetration of the 6^3 net of **1** by the $\{Cu(CN)\}_\infty$ chains. (c) The stacking of two-dimensional sheets in **1**. The $\{Cu(CN)\}_\infty$ chains have been omitted for clarity. The copper atoms are large dark spheres; the cyanide atoms are smaller gray spheres; the nitrogen and carbon atoms of the imine ligand are displayed as small white spheres. This scheme has been adopted throughout the figures.

The ribbons are constructed from puckered $\{Cu(CN)\}_\infty$ chains which are linked at the Cu2 sites through a distal linkage to a triply-bridging cyano group of the adjacent ribbon. This interaction results in the construction of the common structural motif, the four-membered $\{Cu_2C_2\}$ or $\{Cu_2N_2\}$ ring which we formulate in general as $\{Cu_2X_2\}$.[35,38,39] Since the

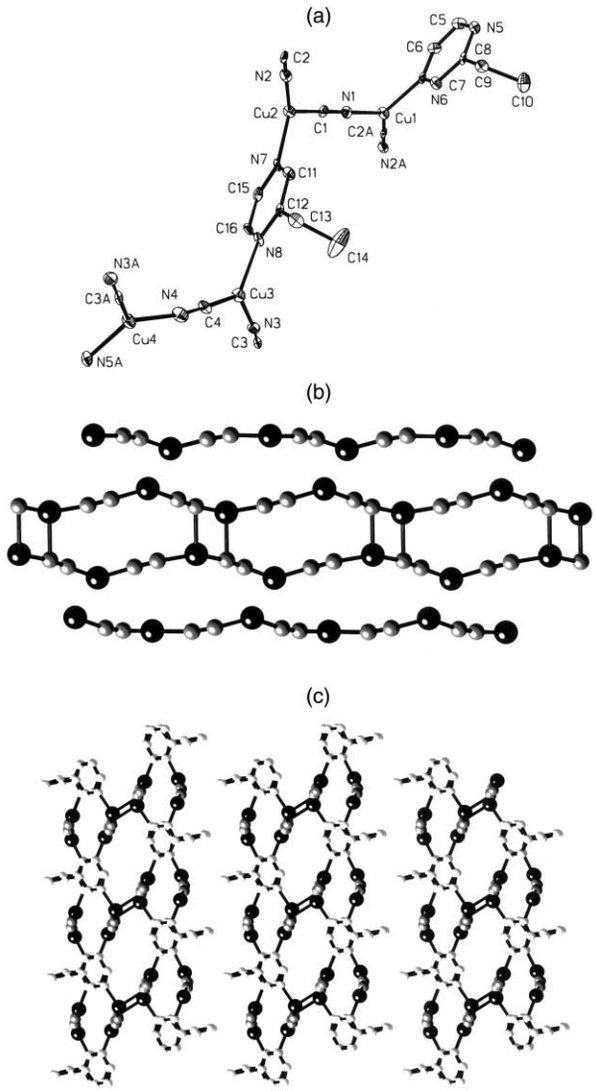

Fig. 2 (a) An ORTEP[40] representation of the asymmetric unit of **2**. (b) The double-stranded ribbon and the chains which provide the building blocks for the network structure. The 12-membered ring dimensions are *ca.* 7.5 Å and 3.5 Å, respectively. (c) The stacking of layers, showing the projection of the ethyl substituents into the interlamellar region.

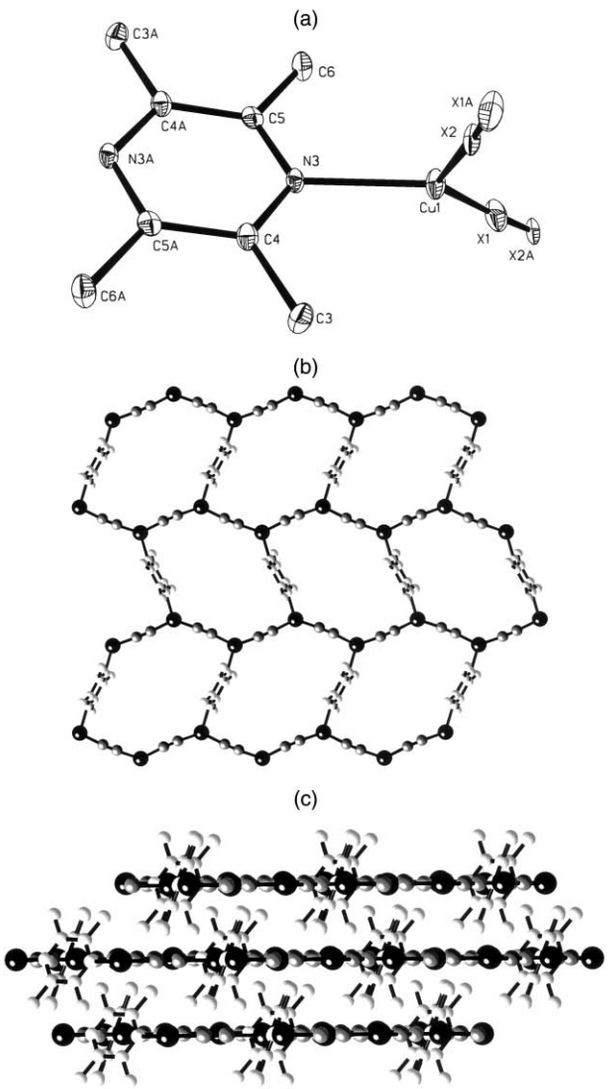

Fig. 3 (a) A view of the asymmetric units of **3**, showing 50% thermal ellipsoids and the atom-labeling scheme. (b) A view of the network structure of **3**. (c) The stacking of layers in **3**.

folding of the chains which comprise the ribbons increases the distance of the Cu1 sites from the adjacent chain of the ribbon, precluding interaction with a cyano group of this chain, a second ring motif appears in the chain, the twelve-membered $\{Cu_4(CN)_4\}$ heterocycle, of approximate dimensions 7.5 × 3.5 Å.

The coordination geometry at the Cu2 site is completed by the N^4 nitrogen of the 2-ethlypyrazine ligand, producing distorted tetrahedral coordination at Cu2. The N^1 site of the ligand (N8) serves to bridge to the Cu3 site of the adjacent $\{Cu(CN)\}_\infty$ chain. The Cu1 centers assume trigonal planar geometries through coordination to the cyano groups of the chain and the N6 site of a 2-ethylpyrazine ligand. The second nitrogen donor of this ligand bridges the ribbon to the Cu4 site of the adjacent chain. Thus, the Cu3 and Cu4 sites of the chain motifs adopt trigonal planar geometries. This connectivity pattern links each ribbon to four adjacent chains and each chain to two adjacent ribbons to form this network. This mode of linkage between chains and ribbons produces a third ring motif $\{Cu_6(CN)_4(etpyr)_2\}$.

The ethyl substituents project into the interlamellar region so as to interdigitate with the substituents from neighboring sheets. The interlamellar distances of 3.0 Å are consistent with the combined van der Waals radii of these substituents. There are no interlayer Cu · · · Cu distances of less than 3.1 Å.

The network structure of $[Cu_2(CN)_2(tmp)]$ (**3**) is topologically identical to that described for the two-dimensional substructure of **1**. The layer of **3**, shown in Fig. 3, is constructed from puckered $\{Cu(CN)\}_\infty$ chains. Each Cu(I) site is coordinated by two bridging cyano groups of the chain and also to a nitrogen donor of the tmp ligand, which generates a distorted trigonal planar geometry at this site. Adjacent chains are linked through the tmp ligands to generate the common 6^3 topology associated with the $\{Cu_6(CN)_4(tmp)_2\}$ rings of the network.

However, the structure of **3** contrasts with that of **1** in an unanticipated fashion, *i.e.*, the absence of the penetrating $\{Cu(CN)\}_\infty$ chain as a substructural unit. It is noteworthy that the Cu · · · Cu distances across the rings are 10.4 Å in **3** and 8.7 Å in **1**. Furthermore, the pyrazine ring in **1** is canted at only 6° with respect to the layer plane, while that in **3** is rotated by *ca.* 70° with respect to the network. As shown in Fig. 3(c), space-filling in the case of **3** is achieved not by introduction of the $\{Cu(CN)\}_\infty$ chain substructure but rather through appropriate stacking of layers, interdigitating the methyl substituents in such a fashion as to align the organic groups of one sheet with the cavities in a neighboring network.

The structures of $[Cu_2(CN)_2(qox)]$ (**4**) and $[Cu_2(CN)_2(phenz)]$ (**5**) are similar to that of **3**. As shown in Fig. 4, $[Cu_2(CN)_2(qox)]$ adopts the common network structure, constructed of

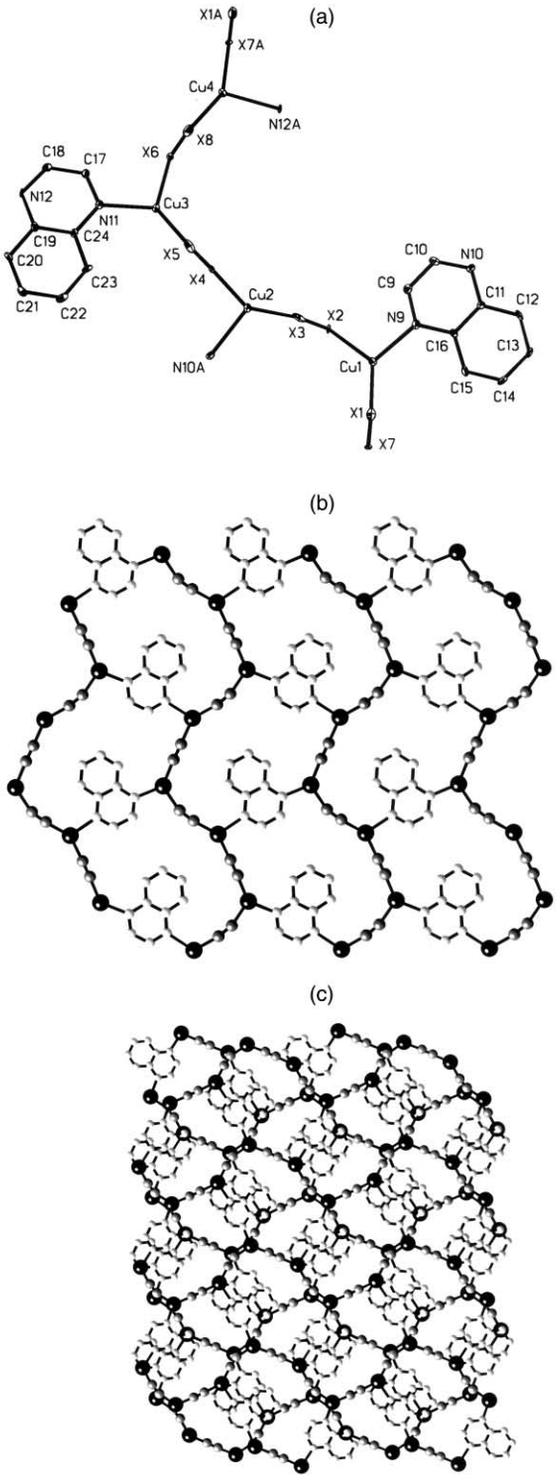

Fig. 4 (a) An ORTEP view of the asymmetric unit of **4**, showing the atom-labeling scheme. (b) A view of the network structure of **4**. (c) The stacking of layers in **4**.

$\{Cu(CN)\}_\infty$ chains linked through quinoxaline ligands into a two-dimensional sheet with the characteristic 6^3 net. However, the $\{Cu(CN)\}_\infty$ chains of **4** are considerably more puckered than those of **3** as a consequence of the orientation of the organic substituent relative to the layer plane. The ligand plane is rotated only *ca.* 8° from the layer plane, requiring the $\{Cu_6(CN)_4(qox)_2\}$ rings to distort to accommodate the sterically demanding substituent. In this case interpenetration is avoided not as a result of blocking the $\{Cu_6(CN)_4L_2\}$ ring cavity through alignment of substituents projecting from adjacent sheets but rather as a consequence of the orientation of substituents within the layer. The interlamellar distance of 3.0 Å reflects 'i-' stacking of the ligands as well as Cu···Cu contacts of 3.032(1) Å.

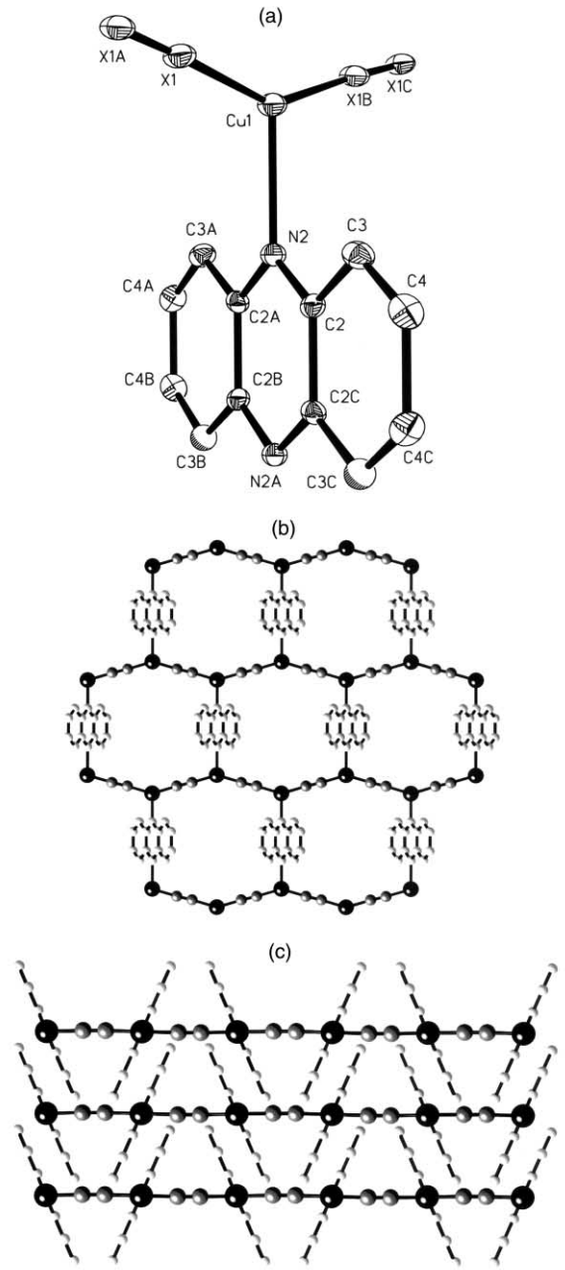

Fig. 5 (a) A view of the structure of **5**, showing the atom-labeling scheme and 50% thermal ellipsoids. (b) A view normal to the plane of **5**. (c) The stacking of networks in **5**.

The structure of the phenazine derivative $[Cu_2(CN)_2(phenz)]$ (**5**) is shown in Fig. 5. Once again this network is constructed from $\{Cu(CN)\}_\infty$ chains linked through the phenazine ligand to produce the common 6^3 topology and $\{Cu_6(CN)_2(phenz)_2\}$ rings. In contrast to the structure of **4**, the plane of the ligand is now canted at 77° with respect to the layer plane. Interdigitation is precluded by the stacking of layers, which in common with the structure of **3**, orients the sterically demanding organic groups to project above and below the ring cavities of adjacent networks.

Perhaps not surprisingly, the structure of $[Cu_7(CN)_7(4,4'\text{-bpy})_2]$ (**6**) is most similar to that of **1**. The structure is constructed from the familiar $\{Cu_2(CN)_2(4,4'\text{-bpy})\}_\infty$ networks and $\{Cu(CN)\}_\infty$ chains which thread through these sheets. The network structure exhibits the characteristic 6^3 topology as shown in Fig. 6. The expansion of the N to N distance in the linear dipodal ligand relative to that in the pyrazine-based

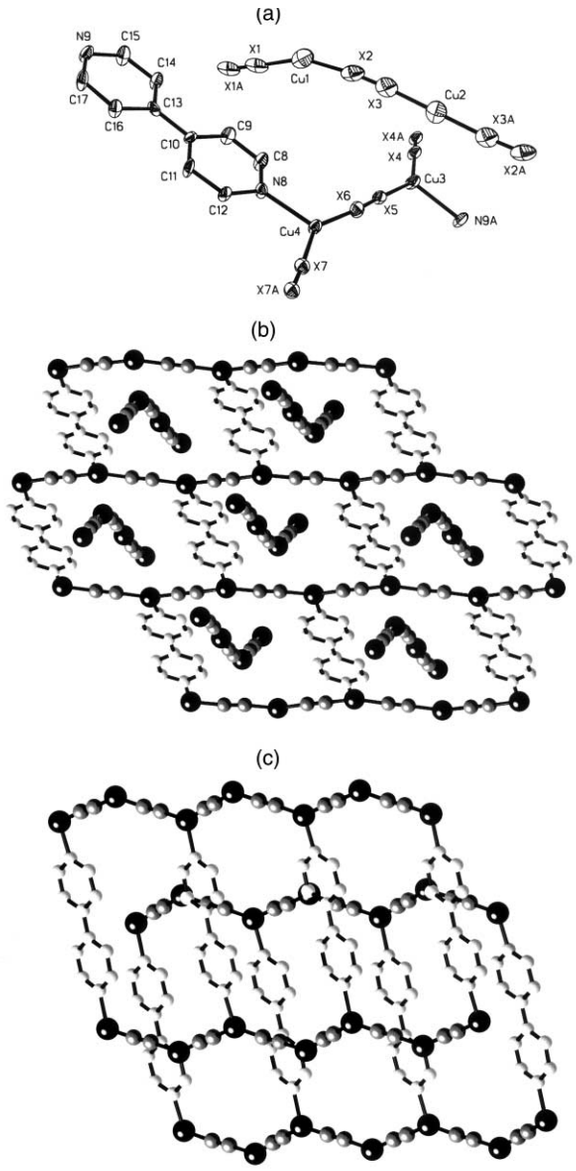

Fig. 6 (a) An ORTEP view of the asymmetric unit of **6**. (b) The network structure of **6**. (c) The stacking of layers in **6**.

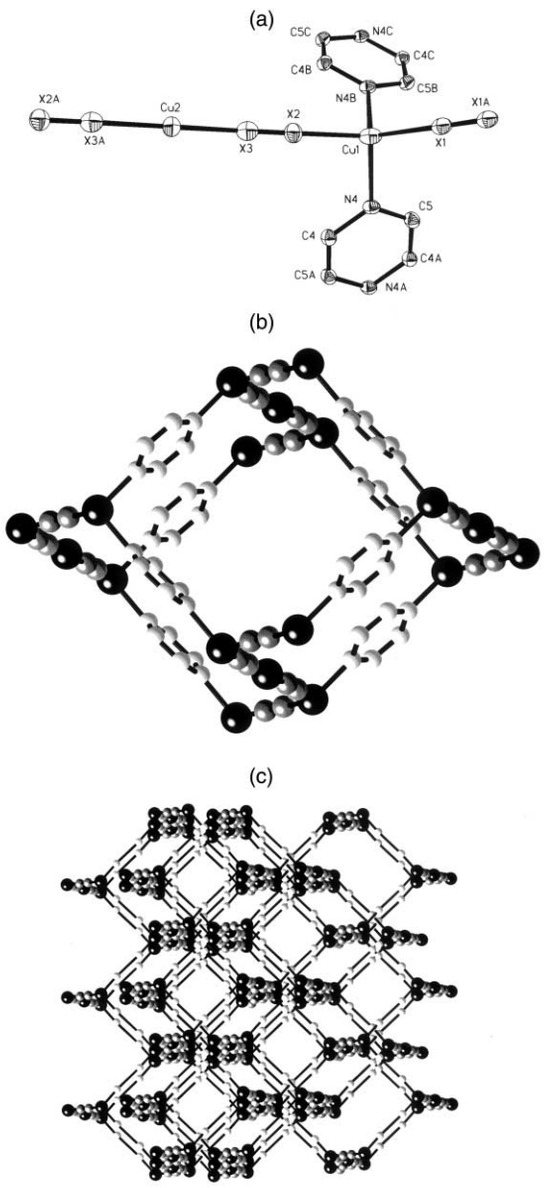

Fig. 7 (a) A view of the copper coordination sites of **7**, showing the atom-labeling scheme and 50% thermal ellipsoids. (b) A view of a section of one three-dimensional framework of **7**. (c) The interpenetration of two equivalent frameworks in **7**.

ligands in **1**–**5** generates a $\{Cu_6(CN)_4(4,4'\text{-bpy})_2\}$ ring with a Cu···Cu dimension of 14.2 Å, compared to 8.7 Å in **1**. This void space readily accommodates the penetrating $\{Cu(CN)\}_\infty$ chain. However, the $\{Cu_2(CN)_2(4,4'\text{-bpy})\}_\infty$ sheets are considerably offset requiring that the {Cu(CN)} chains fold. Consequently, the angle at the two-coordinate Cu1 site is considerably distorted from the linear ideal. The interlamellar distances of 3.0 Å reflect π–π stacking of the ligands and Cu···Cu contacts of 2.950(1) Å. It is also noteworthy that the Cu···Cu distance between Cu1 of the chain and Cu4 of the network is only 2.620(1) Å.

In addition to the $[Cu_3(CN)_3(pyr)]$ (**1**) phase described above, pyrazine reacts with Cu(CN) to produce a three-dimensional phase $[Cu_3(CN)_3(pyr)_2]$ (**7**) shown in Fig. 7. The structure may be described as folded $\{Cu(CN)\}_\infty$ chains linked by pyrazine ligands into a three-dimensional framework. The Cu1 sites of the chain adopt distorted tetrahedral geometry through coordination to two cyano groups of the chain and to two nitrogen donors from two pyrazine ligands. This Cu2 site exhibits linear coordination to two cyanide groups of the chain.

The pyrazine ligands serve to link one chain to four neighboring chains, generating two cyclic substructures $\{Cu_8(CN)_6(pyr)_2\}$ and $\{Cu_6(CN)_2(pyr)_4\}$. The distance between pyrazine linked Cu sites is 6.9 Å. Consequently, as shown in Fig. 7(b), the fusing of cyclic motifs produces box-like substructures encompassing considerable volume. As anticipated, this volume is occupied by a second and identical three-dimensional framework to produce an inextricably interpenetrated structure.

The structures of $[Cu_2(CN)_2(mpyr)]$ (**8**) and $[Cu_2(CN)_2(2,5\text{-dmp})]$ (**10**) are isomorphous. As shown in Fig. 8 for the structure of **10**, the three-dimensional framework is constructed from two common structural motifs, the 6^3 network and double stranded ribbons with the $\{Cu_2X_2\}$ ring substructure. The structure exhibits a single crystallographically unique copper site which exhibits distorted pyramidal geometry through coordination to three cyano groups and the nitrogen donor of the substituted pyrazine.

The 6^3 network exhibits the features common to structures **1** and **3**–**6**: puckered $\{Cu(CN)\}_\infty$ chains linked by 2,5-dmp groups to give a layer constructed of fused $\{Cu_6(CN)_4(2,5\text{-dmp})_2\}$ rings. Each copper site of the network engages in a fourth interaction with a cyano ligand of a neighboring network. Consequently, every cyano group bridges two copper sites in a network and a copper site from a neighboring network. This connectivity generates a second set of two-dimensional net-

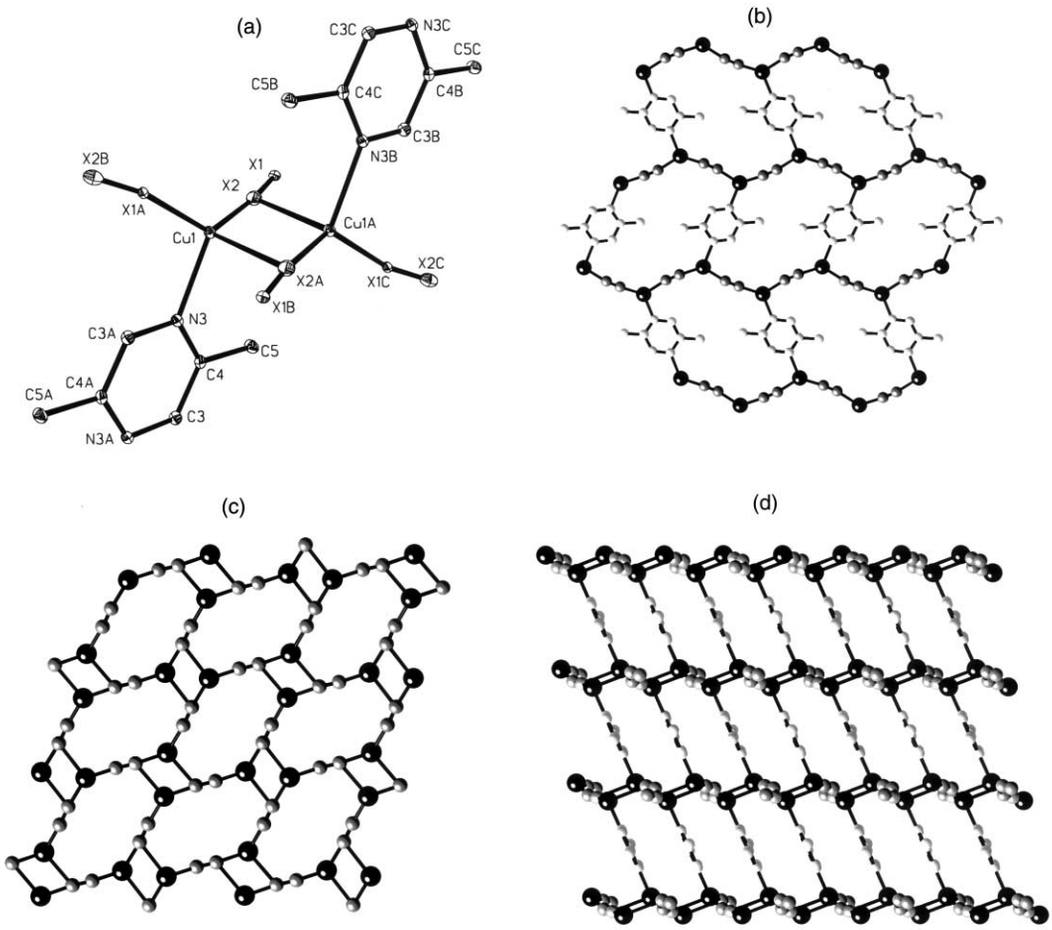

Fig. 8 (a) An ORTEP view of the copper coordination sites in **10**. (b) A view of the 6^3 network substructure of **10**. (c) A view perpendicular to the (100) direction of the network constructed of $\{Cu_2X_2\}$ and $\{Cu_4(CN)_4\}$ rings. (d) A view perpendicular to (010) showing the intersection of networks at the four-coordinate copper centers to produce the overall three-dimensional structure of **10**.

works intersecting the 6^3 motifs at *ca.* 67°, as shown in Figs. 8(c) and 8(d). This $\{Cu(CN)\}_\infty$ network may be described in terms of ribbons of double-stranded $\{Cu(CN)\}_\infty$ chains linked through triply-bridging cyano groups which generate the $\{Cu_2X_2\}$ cyclic motif. In addition to this common structural building block, this network exhibits $\{Cu_4(CN)_4\}$ rings as building blocks. The overall structure may be alternatively described as these $\{Cu(CN)\}_\infty$ networks, stacked along the crystallographic *a*-axis and bridged through the 2,5-dmp ligands [Fig. 8(d)].

The three-dimensional structure of$[Cu_2(CN)_2(2,3\text{-dmp})]$ (**9**) is quite distinct from those associated with $[Cu_3(CN)_3(pyr)_2]$ (**7**) and $[Cu_2(CN)_2(2,5\text{-dmp})]$ (**10**). In this case, as shown in Fig. 9, the structure is constructed from $\{Cu(CN)\}_\infty$ ribbons linked through 2,3-dimethylpyrazine ligands into a three-dimensional framework. The ribbon consists of two $\{Cu(CN)\}_\infty$ puckered chains which are linked through the triply-bridging cyano groups at copper sites Cu3 and Cu4. This connectivity pattern once again generates the common $\{Cu_2X_2\}$ cyclic motif. The second building block of the ribbon is a $\{Cu_6(CN)_6\}$ ring of dimensions 12.6 × 4.4 Å. The $\{Cu_2X_2\}$ and $\{Cu_6(CN)_6\}$ rings fuse in an alternating pattern to form the ribbon. The ribbon substructure of **9** is reminiscent of that encountered in **2**. However, the large ring of **9** $\{Cu_6(CN)_6\}$ has been expanded by two additional $\{Cu(CN)\}$ units in comparison to the $\{Cu_4(CN)_4\}$ motif exhibited by **2**, which has dimensions of 7.5 × 3.5 Å.

There are two distinct copper environments within the ribbons. The Cu3 and Cu4 sites are in distorted tetrahedral geometries, defined by three cyano ligands and a nitrogen donor of the 2,3-dimethylpyrazine ligand. In contrast, sites Cu1, Cu2, Cu5 and Cu6 exhibit trigonal geometries through coordination to two cyano ligands and a nitrogen of a 2,3-dmp ligand. The 2,3-dmp ligands connect a ribbon to four neighboring ligands to produce a three-dimensional framework. A second independent framework interpenetrates the first to produce a doubly interpenetrated structure type.

The structure of $[Cu_2(CN)_2(2,6\text{-dmp})]$ (**11**) is also constructed of double stranded ribbons linked through the substituted pyrazine ligands into a three-dimensional framework. In this case, the ribbon topology is that previously encountered for **2**, constructed from fusing $\{Cu_2X_2\}$ rings and $\{Cu_4(CN)_4\}$ rings. The 2,6-dmp units link a ribbon to four adjacent ribbons to produce the three-dimensional framework. The structures of **2** and **11** differ in several important features. The ribbons in **11** are bridged by the substituted pyrazine to adjacent ribbons, establishing an overall three-dimensional framework. In the case of **2**, each ribbon links to two chains, which prevents extension along the third dimension. This appears to be a consequence of the increased steric constraints associated with the ethyl substituent of **2**, which projects into the interlamellar void. From Fig. 10(b), it is apparent that an ethyl group could not be accommodated in the bridging mode adopted by the ligands in structure **11**.

The structure of $[Cu_2(CN)_2(4,4'\text{-bpy})]$ (**12**) Fig. 11 is most similar to that of $[Cu_2(CN)_2(2,5\text{-dmp})]$ (**10**), in that the three-dimensional framework is constructed from the intersection of two-dimensional network substructures. Two distinct copper coordination geometries contribute to the connectivity pattern. The Cu1 site is distorted tetrahedral through bonding to three cyano ligands and a nitrogen donor of the 4,4′-bipyridyl ligand. The Cu2 site adopts a distorted trigonal geometry defined by

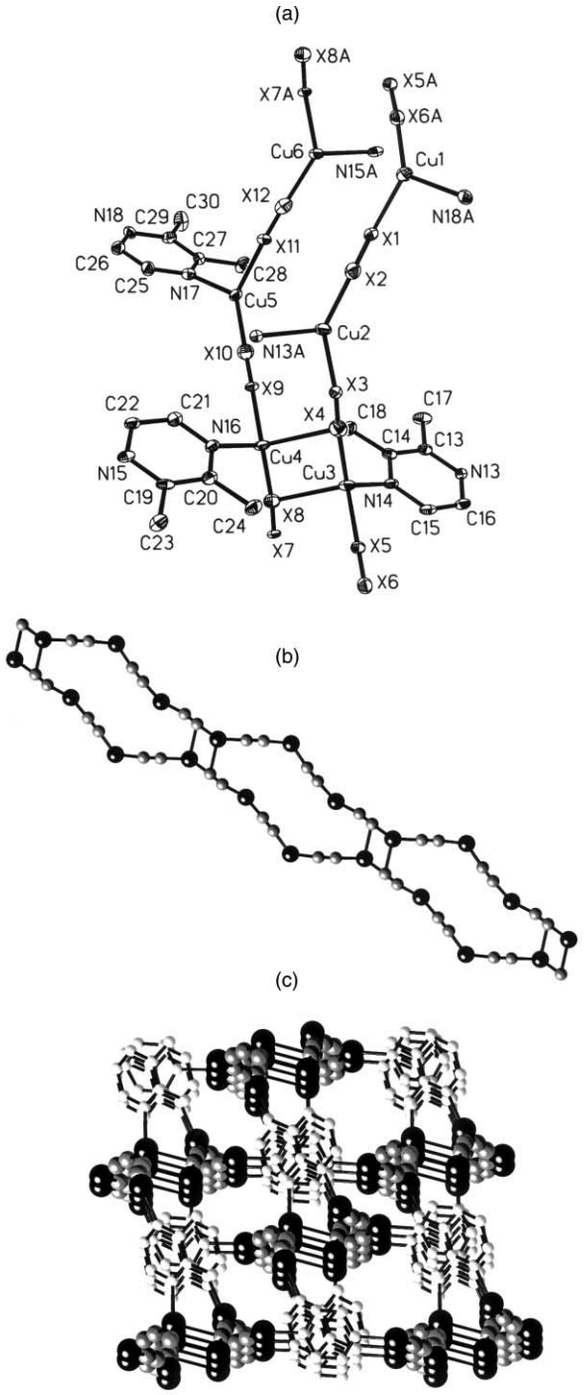

Fig. 9 (a) The atom-labeling scheme and 50% thermal ellipsoids for the metal sites of **9**. (b) A view of the ribbon motif of **9**. (c) The linking of ribbons to produce the three-dimensional structure of **9**.

two cyano ligands and the N5 nitrogen of the 4,4′-bpy. This pattern generates two common network substructures. As shown in Fig. 11, the first, a $\{Cu(CN)\}_\infty$ sheet, is constructed from the common $\{Cu_2X_2\}$ rings fused to $\{Cu_8(CN)_8\}$ rings. However, the rhombic $\{Cu_8(CN)_8\}$ rings of **12** are considerably larger than the $\{Cu_4(CN)_4\}$ rings of **10**, with dimensions of 11.7 × 7.2 Å for **11** compared to 7.7 × 4.6 Å for **10**. The copper site of this network is additionally bound to 4,4′-bipyridyl ligands which project above and below the sheet to link adjacent networks into a three-dimensional structure. Consequently, there is also a $\{Cu_2(CN)_2(4,4'\text{-bpy})\}$ network substructure which intersects the copper cyanide substructure, in a fashion reminiscent of $[Cu_2(CN)_2(2,5\text{-dmp})]$ (**10**). This second network exhibits the common 6^3 motif with $\{Cu_6(CN)_4(4,4'\text{-bpy})_2\}$ rings.

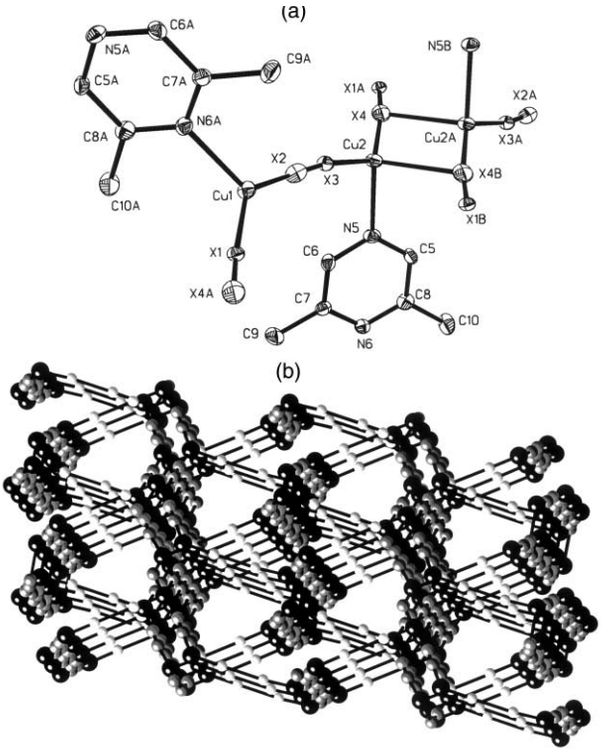

Fig. 10 (a) An ORTEP view of the copper coordination sites in **11**. (b) The linking of ribbons in **11** to generate the framework structure. Only the nitrogen atoms of the 2,6-dmp ligands are shown for clarity.

A significant difference between the structures of **10** and **12** is the dimensions of the cyclic building blocks. Thus, compound **10** exhibits $\{Cu_4(CN)_4\}$ and $\{Cu_6(CN)_4(2,5\text{-dmp})_2\}$ rings, while **12** presents $\{Cu_8(CN)_8\}$ and $\{Cu_6(CN)_4(4,4'\text{-bpy})_2\}$ rings. The consequences of this ring expansion are quite evident in the overall structures of **10** and **12**. In contrast to **10** which exhibits a single three-dimensional framework, the structure of **12** contains two identical non-intersecting but interpenetrating frameworks.

Further expansion of the N to N donor distance of the organodiimine ligand was achieved by substituting *trans*-4,4′-dipyridylethylene for 4,4′-bipyridine. The structural consequences are not totally predictable. The structure of $[Cu_2(CN)_2(dpe)]$ (**13**), shown in Fig. 12, is similar to that of **12** and of **10** in that copper cyanide networks are linked by *trans*-4,4′-dipyridylethylene ligands to form the three-dimensional framework. Likewise, there are two copper geometries: the trigonal Cu1 site, defined by two cyano ligands and a nitrogen of the dpe, and a distorted tetrahedral Cu2 site, defined by three cyano ligands and a nitrogen of the dpe.

The copper cyanide network shown in Fig. 12 is constructed from the common $\{Cu_2X_2\}$ rings and $\{Cu_8(CN)_8\}$ rings. However, it is noteworthy that the $\{Cu_8(CN)_8\}$ rings of **13** are structurally distinct from those of **12**. In **12**, the $\{Cu_2(CN)_2\}$ rings at the corners of the $\{Cu_8(CN)_8\}$ rhomb are linked by Cu sites along all four edges. This arrangement produces rings of dimensions 11.7 × 7.2 Å, and the rings fuse in an alternating long–short pattern in the sheet. In contrast, in the case of **12**, the $\{Cu_2(CN)_2\}$ rings are fused along a common cyano group at two opposite edges of the $\{Cu_8(CN)_8\}$ ring and bridged by $\{Cu_2(CN)\}$ units along the remaining edges, producing a cavity of dimensions 12.9 × 16.7 Å. In the structure of **12**, the long and short edges are aligned to avoid the herringbone pattern of **10**. Quite predictably, the large void spaces in the three-dimensional $[Cu_2(CN)_2(dpe)]$ framework results in interpenetration by a second independent framework, as shown in Fig. 12.

Table 15 Summary of structural characteristics for the Cu(I)–cyanide–organodiimine complexes of this study

Compound	Overall covalent connectivity	Cu cyanide substructures[a]	Cyclic motifs Cu–cyanide	Cu–cyanide–LL[b]	Threading or interpenetration
$[Cu_3(CN)_3(pyr)]$ (**1**)	1-D/2-D	Chains	—	$\{Cu_6(CN)_4(LL)_2\}$	Yes
$[Cu_2(CN)_2(etpyr)]$ (**2**)	2-D	Chains	$\{Cu_2X_2\}$	$\{Cu_6(CN)_4(LL)_2\}$	No
		Ribbons	$\{Cu_4(CN)_4\}$		
$[Cu_2(CN)_2(tmp)]$ (**3**)	2-D	Chains	—	$\{Cu_6(CN)_4(LL)_2\}$	No
$[Cu_2(CN)_2(qox)]$ (**4**)	2-D	Chains	—	$\{Cu_6(CN)_4(LL)_2\}$	No
$[Cu_2(CN)_2(phenz)]$ (**5**)	2-D	Chains	—	$\{Cu_6(CN)_4(LL)_2\}$	No
$[Cu_7(CN)_7(4,4'\text{-bpy})_2]$ (**6**)	1-D/2-D	Chains	—	$\{Cu_6(CN)_4(LL)_2\}$	Yes
$[Cu_3(CN)_3(pyr)_2]$ (**7**)	3-D	Chains	—	$\{Cu_8(CN)_6(LL)_2\}$	Yes
$[Cu_2(CN)_2(mpyr)]$ (**8**)	3-D	Chains	$\{Cu_2X_2\}$	$\{Cu_6(CN)_4(LL)_2\}$	No
		Sheets	$\{Cu_4(CN)_4\}$		
$[Cu_2(CN)_2(2,3\text{-dmp})]$ (**9**)	3-D	Ribbons	$\{Cu_2X_2\}$	$\{Cu_6(CN)_4(LL)_2\}$	No
			$\{Cu_6(CN)_6\}$		
$[Cu_2(CN)_2(2,5\text{-dmp})]$ (**10**)	3-D	Chains	$\{Cu_2X_2\}$	$\{Cu_6(CN)_4(LL)_2\}$	No
		Sheets	$\{Cu_4(CN)_4\}$		
$[Cu_2(CN)_2(2,6\text{-dmp})]$ (**11**)	3-D	Ribbons	$\{Cu_2X_2\}$	$\{Cu_8(CN)_6(LL)_2\}$	No
			$\{Cu_4(CN)_4\}$		
$[Cu_2(CN)_2(4,4'\text{-bpy})]$ (**12**)	3-D	Chains	$\{Cu_2X_2\}$	$\{Cu_6(CN)_4(LL)_2\}$	Yes
		Sheets	$\{Cu_8(CN)_8\}$		
$[Cu_2(CN)_2(dpe)]$ (**13**)	3-D	Chains	$\{Cu_2X_2\}$	$\{Cu_6(CN)_4(LL)_2\}$	Yes
		Sheets	$\{Cu_8(CN)_8\}$		

[a] Ribbons and sheets $\{Cu(CN)\}_\infty$ may be considered in terms of fused chains. Consequently, all ribbon and sheet motifs contain chain substructures. The Cu cyanide substructure column lists chains only in those cases where the chains are independent of the $\{Cu(CN)\}_\infty$ sheet or ribbon. [b] LL = Organodiimine.

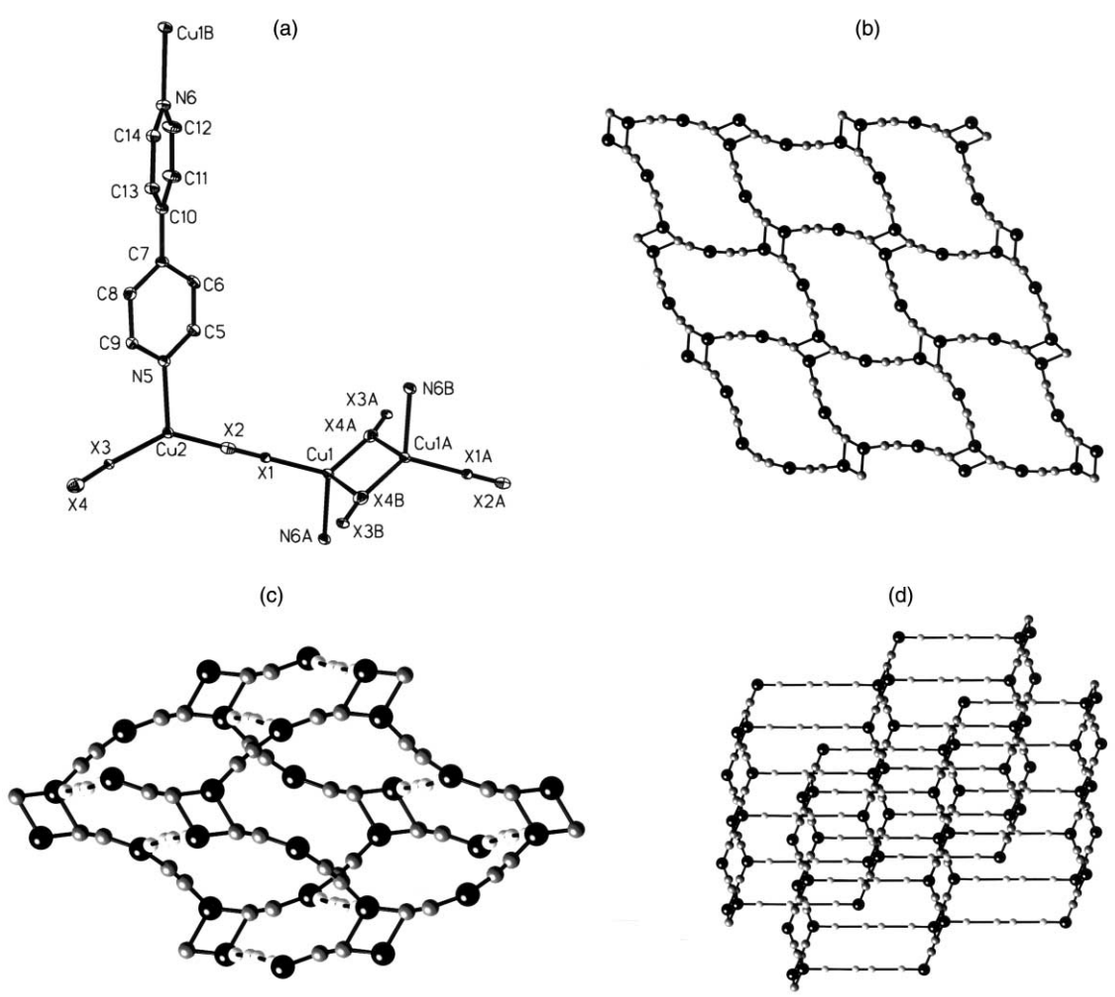

Fig. 11 (a) The atom-labeling scheme and 50% thermal ellipsoids for **12**. (b) The copper cyanide network of **12**, showing the $\{Cu_2X_2\}$ and $\{Cu_8(CN)_8\}$ rings. (c) The linking of the networks shown in (b) through 4,4′-bpy ligands (non-bridgehead carbon atoms of the 4,4′-bpy omitted for clarity). (d) The independent interpenetrating frameworks of **12**. Only the nitrogen, C4 and C4′ atoms of the bpy ligand are shown.

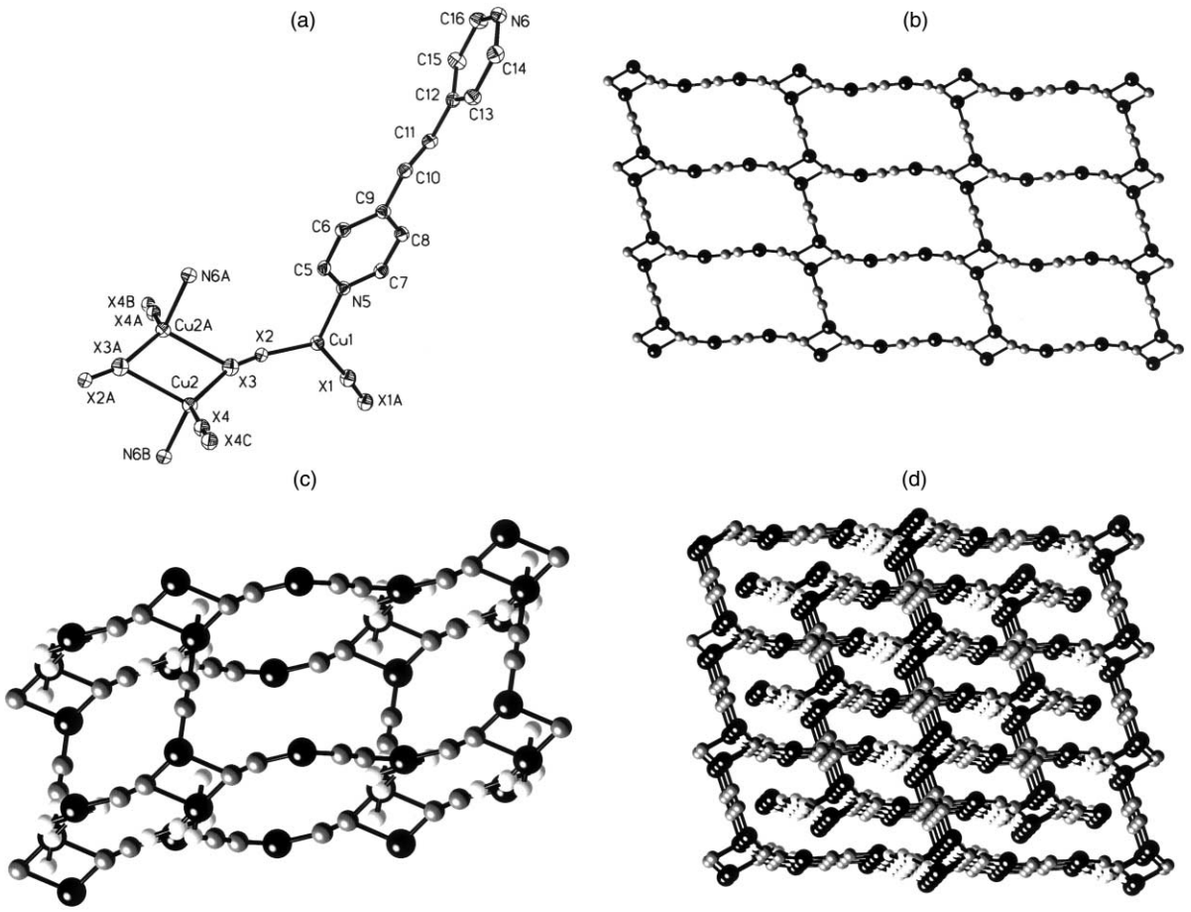

Fig. 12 (a) A view of the metal coordination sites in **13**, showing the atom-labeling scheme and 50% thermal ellipsoids. (b) The copper cyanide network of **13**, illustrating the $\{Cu_2X_2\}$ rings and the $\{Cu_8(CN)_8\}$ rings. (c) The linking of copper cyanide networks through 4,4′-dpe bridges. (d) A view of the interpenetration.

Discussion

While the structural descriptions of **1**–**13** presented above appear to provide a dismaying diversity of characteristics, certain systematics are manifested when the structures are considered in terms of persistent building blocks. This approach is summarized in Table 15 which tabulates the dimensionalities, substructural motifs and presence or absence of interpenetration for the structures of this study.

We first draw attention to the presence of some form of one-dimensional $\{Cu(CN)_3\}_\infty$ chains in all structures. These may be present as isolated chains, as in **1** and **6**; as chains linked through the bridging organodiimine ligands, which occurs in all cases; or as chains fused into ribbons in **2**, **9** and **11** or into sheets in **8**, **10**, **12** and **13**. This observation is not totally surprising since [Cu(CN)] itself exhibits a one-dimensional chain structure,[9] which suggests solubilization of $\{Cu(CN)\}_x$ units under hydrothermal conditions, followed by condensation into chains, ribbons or sheets. However, there is as yet no direct experimental evidence for such preorganization in the reaction media.

In considering the two-dimensional structures **1**–**6**, we note that all contain the $\{Cu_6(CN)_4(LL)_2\}$ cyclic motif as a building block, a motif which persists into the three-dimensional phases **8**–**10**, **12**, and **13**. This cyclic substructure apparently reflects the linear disposition of the donor groups and the coordination preferences of the Cu(I) sites. Assuming that one-dimensional $\{Cu(CN)\}_\infty$ chains provide the structural backbone for materials of the Cu(I)–cyanide–organoimine family, the linking of chains requires expansion of the Cu(I) coordination number and a geometry suitable for structural expansion in two dimensions. Trigonal geometry at Cu(I) centers is common and readily accommodates connectivity between $\{Cu(CN)\}_\infty$ chains. However, when organodiimine groups are placed on adjacent Cu(I) sites of the chain, steric considerations dictate that the ligands on neighboring Cu(I) centers project to opposite sides of the chain. The structural growth in two dimensions then provides the common 6^3 grid work associated with the structures of this study. However, it should be noted that organopolyimine ligands with nonlinear disposition of donor groups will give rise to quite different cyclic motifs in two-dimensional structures. For example, in $[Cu_3(CN)_2(triazolate)_2(bpy)]$, $\{Cu_4(CN)_2(trz)_2\}$ rings are formed, while in $[Cu_5(CN)_3(triazolate)(bpy)]$, $\{Cu_8(CN)_6(trz)_2\}$ and $\{Cu_8(CN)_2(triazolate)_6\}$ rings are observed. In the absence of structural terminating or passivating 2,2′-bipyridyl, the Cu(I)–cyanide–triazolate system also provides $[Cu_6(CN)_5(triazolate)]$, which exhibits $\{Cu_{14}(CN)_{10}(triazolate)_4\}$ rings. It is noteworthy that ligand geometry and denticity can profoundly influence the $\{Cu_x(CN)_y(L)_z\}$ substructure.

The two-dimensional structures may also be distinguished by the presence or absence of threading or interpenetration. Thus, **1** and **6** exhibit two-dimensional networks through which one-dimensional chains are threaded, while this threading is absent in **3**–**5**. This observation appears to reflect the steric influences of the substituents on the pyrazine bridges. Thus, the cavity dimensions of 8.7 × 7.2 Å in the prototypical $[Cu_3(CN)_3(pyr)]$ (**1**) are sufficient to accommodate the $\{Cu(CN)\}_\infty$ chains, as an expedient to fill the potential void volume. Similarly, the spatial extension provided by 4,4′-bpy in **6** expands the cavity to 14.2 × 7.2 Å and allows penetration of the network by the one-dimensional chains.

In structures **3**–**5**, the pyrazine substituents would obviously block threading of the networks, were these sterically bulky units in the plane of the network, as pyrazine and 4,4′-bipyridine are in **1** and **6**, respectively. However, minimization of steric interactions between ligand ribbons is encountered in Cu cyanide substructures where the ribbon is constructed from $\{Cu_2X_2\}$ and $\{Cu_4(CN)_4\}$ rings. The $\{Cu_2X_2\}$ motif is found in all the structures of this study which contain ribbons or sheets as Cu(I) cyanide substructures, that is, **2** and **8**–**13**. The $\{Cu_4(CN)_4\}$ ring appears in **2** and **8**–**11**, but **12** and **13** curiously exhibit an expanded $\{Cu_8(CN)_8\}$ motif. However, it is noteworthy that considerable variability has been observed in such $\{Cu(CN)\}_n$ cyclic building blocks. For example, void volume is achieved by rotating the ligands in **3**–**5** nearly perpendicular to the network. While the cavities in the grid are now putatively accessible, threading is precluded by the stacking arrangement of sheets which align so as to nestle the pyrazine substituents from neighboring layers directly above and below the grid cavities.

The most unusual structure of the family of two-dimensional materials is $[Cu_2(CN)_2(etpyr)]$ (**2**). The ribbon architecture associated with **2** provided considerable flexibility for further structural expansion, since the double strands contain two distinct Cu sites for bridging through the organodiimine ligands. In the case of **2**, a two-dimensional structure is obtained as a result of bridging to $\{Cu(CN)\}_\infty$ chains, which serve to terminate the structural expansion. It would also appear that the structure of **2** is reflective of the steric constraints imposed by the bulky ethyl-substituents. These project from the surfaces of the layers and would seem to preclude expansion in the third dimension. However, the ability of Cu(I) cyanide materials to form large $\{Cu(CN)\}_x$ rings suggests that the need to encompass a large volume occupied by a bulky substituent is not the sole determinant. The partitioning of the structure of **2** into inorganic networks and organic interlamellar domains suggests that the interplay of hydrophobic and hydrophilic interactions may play a dominant role in structural expansion.

The three-dimensional structures, **7**–**13**, exhibit considerable variability, despite the presence of common building blocks. The most obvious characteristic of these phases is the presence or absence of equivalent interpenetrating frameworks. The three structures which contain organodiimines with no bulky substituents **7**, **12** and **13** exhibit interpenetration. Furthermore, **12** and **13** contain organodiimine ligands with spacers between nitrogen donors, providing considerably more framework void space. Consequently, we conclude that the absence of interpenetration in **8**–**11** is a result of steric considerations.

Structures **8**–**13** contain $\{Cu_2X_2\}$ rings as a common structural motif. The exception, compound **7**, shares with **12** and **13** the presence of $\{Cu_8(CN)_6(LL)_2\}$ rings. However, in **12** and **13** these participate with $\{Cu_2X_2\}$ rings in forming two-dimensional sheets, while in **7**, the composite rings fuse to form cages.

The structures of **8**, **10**, **12** and **13** exhibit similar building blocks: Cu(I) cyanide sheets constructed from the fusing of $\{Cu_2X_2\}$ and $\{Cu(CN)\}_n$ ($n = 4$ for **8** and **10**; 8 for **12** and **13**). These sheets are bridged by the organodiimine ligands to produce networks of fused $\{Cu_6(CN)_4(LL)_2\}$ rings which intersect the Cu(I) cyanide layers to form the three-dimensional framework. The $\{Cu_6(CN)_4(LL)_2\}$ network is similar to that observed for the two-dimensional phases **1** and **3**–**6**. Expansion in the third dimension is related to the fusing of $\{Cu(CN)\}_\infty$ chains through $\{Cu_2X_2\}$ interactions to provide the intersecting sheets of the framework. It would appear that the more sterically demanding ligands 2-ethylpyridine, quinoxaline, tetramethylpyridine and phenazine prevent the formation of the intersecting $\{Cu(CN)\}_\infty$ network due to steric constraints. The less demanding 2-methylpyridine and 2,3-, 2,5- and 2,6-dimethylpyrazine allow structural propagation and framework formation. It is noteworthy that the sterically "innocent" pyrazine and 4,4′-bipyridine form both two- and three-dimensional phases. However, the two-dimensional materials exhibit networks threaded by $\{Cu(CN)\}_\infty$ chains, while the three-dimensional structures are interpenetrated. Both structure types are consistent with absence of substituent imposed steric constraints. In the case of **13**, the absence of the corresponding two-dimensional phase $[Cu_7(CN)_7(dpe)_2]$ suggests that the expansion of void space is so significant as to demand interpenetration to satisfy crystal packing requirements. However, the failure to isolate the phase may simply reflect that the appropriate synthetic conditions were not accessed.

As noted for the structure of **2**, the phases constructed from $\{Cu(CN)\}_\infty$ ribbons exhibit the most unusual characteristics. The structures of **9** and **11** contain the same ribbon building block as **2**, but in these instances the bridging organodiimine ligands link a given ribbon to four adjacent ribbons to produce the three-dimensional structure. The structures of **8** and **10** are profoundly different from those of **9** and **11**. The sheet motifs of **8** and **10** can be considered to be constructed from the ribbon building blocks by fusion of the ribbons. While the geometric relationship is apparent, it is not at all clear what influence the identity of the ligand exerts in structural propagation.

Conclusions

A series of novel and complex structure types of the copper–cyanide–organodiimine family have been isolated from hydrothermal media and structurally characterized. The results reinforce the observation that hydrothermal chemistry offers an effective synthetic tool for the isolation of composite organic–inorganic materials. It is also clear that organic ligands with specific geometric requirements may be introduced as structural components of materials. Bridging ligands may be used to propagate the architecture about a metal site, while the steric influences of substituents may be exploited to dictate the dimensionality of the product. Manipulation of the microstructure of the solid is thus achieved by tuning the coordination influences of the metal to the geometric requirements of the ligand.

Two structural subsets have been identified; the two-dimensional phases **1**–**6** and the three-dimensional materials **7**–**13**. The failure to propagate structures **2**–**5** in the third dimension is apparently a consequence of the steric constraints of the ligands. In the cases of **1** and **6**, the networks are threaded by one-dimensional substructures, an observation consistent with the relief of steric requirements for these phases.

Steric influences are also observed for the three-dimensional materials. Sterically "innocent" ligands provide materials with interpenetrating framework structures, while more bulky ligands result in single framework structures.

While it is now evident that organic components may be introduced into the synthesis of solid state inorganic materials in order to manipulate the coordination chemistry of the metal and consequently the structure of the material, designed extended structures remain elusive in the sense of predictability of the final structure. However, this observation reflects the compositional and structural versatility of inorganic materials and should be considered an opportunity for development rather than an occasion for lamentation. The subtle interplay of metal oxidation states, coordination preferences, polyhedral variability, ligand donor groups, types, and orientations, spatial extension, and steric constraints provides a limitless set of construction components for solid state materials. As the products of empirical observations are elucidated, the structure–function relationships of such components will begin to emerge and to provide further guidelines for synthetic methodologies.

Acknowledgements

This work was supported by a grant from the National Science Foundation (CHE 9987471) and the W. M. Keck Foundation. We wish to thank Dr. Charles Campana of Bruker Instruments for his assistance in the solution and refinement of structure **1**.

References

1 T. Iwamoto, in *Comprehensive Supramolecular Chemistry*, ed. D. D. MacNicol, F. Toda and R. Bishop, Permagon Press, Oxford, 1996, vol. 6, ch. 19, p. 643.
2 K. R. Dunbar and R. A. Heintz, *Prog. Inorg. Chem.*, 1997, **45**, 283.
3 T. Iwamoto, *J. Inclusion Phenom.*, 1996, **4**, 61.
4 C. Janiak, *Angew. Chem., Int. Ed. Engl.*, 1997, **36**, 1431 and references therein.
5 B. F. Hoskins and R. Robson, *J. Am. Chem. Soc.*, 1990, **112**, 1846.
6 W. P. Fehlhammer and M. Fritz, *Chem. Rev.*, 1993, **93**, 1243.
7 S.-W. Zhang, D.-G. Fu, W.-Y. Sun, Z. Hu, K.-B. Yu and W.-X. Tang, *Inorg. Chem.*, 2000, **39**, 1142 and references therein.
8 S. Ferlay, T. Malleh, R. Ouakès, P. Veillet and M. Verdaguer, *Nature*, 1995, **378**, 701.
9 S. Kroeker, R. E. Wasylishen and J. V. Hanna, *J. Am. Chem. Soc.*, 1999, **121**, 1582.
10 B. H. Lipshutz, J. A. Sclafan and T. Takanami, *J. Am. Chem. Soc.*, 1998, **120**, 4021.
11 L. C. Brousseau, D. Williams, J. Kouvetakis and M. O'Keefe, *J. Am. Chem. Soc.*, 1997, **119**, 6292.
12 D. J. Chesnut and J. Zubieta, *Chem. Commun.*, 1998, 1707.
13 D. J. Chesnut, A. Kusnetzow and J. Zubieta, *J. Chem. Soc., Dalton Trans.*, 1998, 4081.
14 D. J. Chesnut, A. Kusnetzow, R. R. Birge and J. Zubieta, *Inorg. Chem.*, 1999, **38**, 2663.
15 D. J. Chesnut, A. Kusnetzow, R. Birge and J. Zubieta, *Inorg. Chem.*, 1999, **38**, 5484.
16 N. A. Khan, N. Baber, M. Z. Iqbal and M. Mazhar, *Chem. Mater.*, 1993, **5**, 1283.
17 S. R. Batten and R. Robson, *Angew. Chem., Int. Ed.*, 1998, **37**, 1460 and references therein.
18 Some representative references from leading researchers in the field of coordination polymers: (*a*) M. J. Zaworotko, *Chem. Soc. Rev.*, 1994, **23**, 283; (*b*) H. Gudbjartson, K. Biradha, K. M. Poirier and M. J. Zaworotko, *J. Am. Chem. Soc.*, 1999, **121**, 2599; (*c*) B. F. Abrahams, P. A. Jackson and R. Robson, *Angew. Chem., Int. Ed.*, 1998, **37**, 2656; (*d*) L. Carlucci, G. Ciani, D. M. Proserpio and A. Sironi, *Inorg. Chem.*, 1998, **37**, 5941; (*e*) O. M. Yaghi, H. Li, C. Davis, D. Richardson and T. L. Groy, *Acc. Chem. Res.*, 1998, **31**, 474; (*f*) S. Lopez and S. W. Keller, *Inorg. Chem.*, 1999, **38**, 1883; (*g*) M. Kondo, T. Okubo, A. Asami, S. Noro, T. Yoshitomi, S. Kitagawa, T. Ishii, H. Matsuzaka and K. Seki, *Angew. Chem., Int. Ed.*, 1999, **38**, 140; (*h*) D. M. L. Goodgame, D. A. Grachvogel and D. J. Williams, *Angew. Chem., Int. Ed.*, 1999, **38**, 153; (*i*) C. V. K. Sharma and R. D. Rogers, *Chem. Commun.*, 1999, 83; (*j*) M. Fujita, Y. J. Kwon, S. Washizu and K. Ogura, *J. Am. Chem. Soc.*, 1994, **116**, 1151; (*k*) M. A. Withersby, A. J. Blake, W. R. Champness, P. Hubberstey, W.-S. Li and M. Schröder, *Angew. Chem., Int. Ed. Engl.*, 1997, **37**, 2327; (*l*) A. J. Blake, S. J. Mill, P. Hubberstey and W.-S. Li, *J. Chem. Soc., Dalton Trans.*, 1998, 909; (*m*) J. S. Moore and S. Lee, *Chem. Ind. (London)*, 1994, **14**, 556; (*n*) A. Mayr and J. Guo, *Inorg. Chem.*, 1999, **38**, 921.
19 O. Teichert and W. S. Sheldrick, *Z. Anorg. Allg. Chem.*, 1999, **625**, 1860.
20 B. Rossenbeck and W. S. Sheldrick, *Z. Naturforsch., Teil B*, 1999, **54**, 1510.
21 Siemens SMART Software Reference Manual, Siemens Analytical X-Ray Instruments, Inc., Madison, Wisconsin, 1994.
22 G. M. Sheldrick, SADABS, Program for Empirical Absorption Corrections, University of Göttingen, Germany, 1996.
23 G. M. Sheldrick, SHELXL96, Program for the Refinement of Crystal Structures, University of Göttingen, Germany, 1996.
24 J. Gopalakrishnan, *Chem. Mater.*, 1995, **7**, 1265.
25 A. Stein, S. W. Keller and T. E. Mallouk, *Science*, 1993, **257**, 1558.
26 D. J. Chesnut, D. Hagrman, P. J. Zapf, R. P. Hammond, R. LaDuca, Jr., R. C. Haushalter and J. Zubieta, *Coord. Chem. Rev.*, 1999, **190–192**, 757.
27 D. Hagrman, P. J. Zapf and J. Zubieta, *Angew. Chem., Int. Ed.*, 1999, **38**, 3165.
28 A. G. Sharpe, *The Chemistry of Cyano Complexes of the Transition Metals*, Academic Press, New York, 1976.
29 D. Cooper and R. A. Plane, *Inorg. Chem.*, 1996, **5**, 2209.
30 J. K. Burdett and O. Eisenstein, *Inorg. Chem.*, 1992, **31**, 1758.
31 G. A. Bowmaker, H. Hartl and V. Urban, *Inorg. Chem.*, 2000, **39**, 4548.
32 D. T. Cromer, *J. Phys. Chem.*, 1957, **61**, 1388.
33 C. Kappenstein and R. P. Hugel, *Inorg. Chem.*, 1977, **16**, 250.
34 D. T. Cromer and A. C. Larson, *Acta Crystallogr.*, 1962, **15**, 397.
35 F. B. Stocker, T. P. Staeve, C. M. Rienstra and D. Britton, *Inorg. Chem.*, 1999, **38**, 984.
36 A. F. Wells, *Three-Dimensional Nets and Polyhedra*, Wiley-Interscience, New York, 1977.
37 R. Kuhlman, G. L. Schimek and J. W. Kolis, *Polyhedron*, 1999, **18**, 1379.
38 D. T. Cromer, A. C. Larson and R. B. Roof, Jr., *Acta Crystallogr.*, 1965, **19**, 192.
39 J. D. Kildea, B. W. Skelton and A. H. White, *Aust. J. Chem.*, 1985, **38**, 1329.
40 C. K. Johnson, ORTEP, Report ORNL-5138, Oak Ridge National Laboratory, Oak Ridge, TN, 1976.